Quarterly Journal of the
Royal Meteorological Society

Annual Cycle of the West African Monsoon - Regional Circulations and Associated Water Vapor Transport

Journal:	*QJRMS*
Manuscript ID:	QJ-09-0234.R1
Wiley - Manuscript type:	Research Article
Date Submitted by the Author:	n/a
Complete List of Authors:	Thorncroft, Chris; University at Albany, Department of Atmospheric and Environmental Sciences Nguyen, Hanh; University at Albany, Department of Atmospheric and Environmental Sciences Zhang, Chidong; University of Miami, Division of Meteorology and Physical Oceanography Peyrille, philippe; Meteo france
Keywords:	rainfall, onset, moisture flux, heat low, cold tongue

Annual Cycle of the West African Monsoon - Regional Circulations and Associated Water Vapor Transport

Chris D. Thorncroft, Hanh Nguyen
Department of Atmospheric and Environmental Sciences, University at Albany, SUNY, New York

Chidong Zhang
RSMAS, University of Miami, Miami, Florida

Philippe Peyrillé
Météo France, Paris

Abstract

Analysis of the annually varying regional circulations and their relationship to surface conditions and water vapor transport in the West African region is presented. The progression of the West African monsoon is described in terms of four key phases: (i) An *oceanic phase* between November and mid-April when the rainband is broad with peak values just north of the Equator (~1^{o}N); (ii) A *coastal phase* between mid-April and the end of June when the rainfall peak is in the coastal region around 4^{o}N (over the ocean); (iii) A *transitional phase* during the first half of July when the rainfall peak decreases and (iv) A *Sahelian phase* between mid-July and September when the rainfall peak is more intense and established in the Sahelian region around 10^{o}N. The annual evolution of the moisture fluxes, associated convergence, and rainfall is strongly impacted by the Atlantic cold tongue (cool water close to the equator between Boreal Spring and Summer) and the Saharan heat low. The cold tongue strongly regulates the timing and intensity of the coastal rainfall in spring. The heat low and its associated shallow meridional circulation strongly affect the profile in moisture flux convergence north of the main rainband maximum; in particular it is responsible for the establishment of a second peak in column moisture flux convergence there (approximately 8^{o} poleward of the rainfall peak).

Particular emphasis is given to the coastal rainfall onset in April. A key aspect of this onset is acceleration of low-level cross-equatorial southerly winds, important for establishing the cold tongue, discouraging convection near the equator and transporting moisture towards the coast. We argue that the rainfall peak is maintained at the coast,

rather than steadily moving inland with the solar insolation, due to persistent warm water in the coastal region together with frictionally induced moisture convergence there.

Keywords: rainfall, onset, moisture flux, cold tongue, heat low

1. Introduction

The West African monsoon (WAM) has a distinctive annual cycle in rainfall that remains a challenge to understand and predict (e.g. Cook and Vizy, 2006). The location of peak rainfall, which resides in the northern hemisphere throughout the year, moves from the ocean to the land in boreal Spring (e.g. Okumura and Xie, 2004). Around the end of June there is a rapid shift in the location of peak rainfall between the coast and around 10^{o}N where it remains until about the end of August (Sultan and Janicot, 2000). In September the peak rainfall returns equatorward in a relatively steady pace and is located over the ocean again by November. The fact that the peak rainfall migrates irregularly compared to the peak solar heating is due to the interactions that occur between the land, the atmosphere and the ocean (e.g. Li and Philander, 1997, Chou et al, 2001, Okumura and Xie, 2004). These interactions take place through the regional circulations connecting the land and the ocean. The purpose of this paper is to explore how the climatological annual cycle of these circulations are related to surface conditions and how they impact the regional transport of water vapour and its convergence.

Fundamentally the WAM arises in association with thermodynamic contrasts between the land and ocean surfaces. Two distinctive meridional overturning circulations characterize the WAM, a deep circulation associated with a gradient in low-level equivalent potential temperature and contrasts in deep moist convection (e.g. Eltahir and Gong, 1997) and a shallow meridional circulation (SMC) associated with a gradient in low-level potential temperature and contrasts in dry convection (Thorncroft and Blackburn, 1990, Nolan et al, 2007, Zhang et al, 2008). While each of these circulations is associated with advection

of moist air from the ocean to the land at low-levels, the SMC is also associated with advection of drier air equatorwards at mid-levels. At the monthly time scale, the moistening at low levels and drying at mid-levels associated with the SMC can have a blocking effect on convection over land (Peyrillé and Lafore, 2007) but the effect during the complete annual cycle is less clear. A detailed description of the role of the different circulations on the regional moisture transports and how this relates to the annual cycle of rainfall in the WAM region is lacking and will be addressed here.

One of the most important studies of the water vapor transport in the WAM region was carried out by Cadet and Nnoli (1987). This study used operational ECMWF analyses to explore the water vapor transport during the summer of 1979. Based on an analysis of bi-weekly averaged fields of water vapor fluxes and associated moisture flux convergence they highlighted the importance of the Gulf of Guinea as a source of moisture for West as well as Central Africa. They also showed that the African easterly jet (AEJ) was associated with significant easterly moisture fluxes. For their region of study, between 10^{o}W and 10^{o}E, the moisture fluxes at this mid-level were divergent which lead the authors to conclude that "the mid-troposphere has little influence on rainfall". While it might be concluded that this drying will not enhance rainfall, it is possible that it may suppress rainfall, so the authors' conclusion that the mid-troposphere has little influence on rainfall requires further investigation including, in particular, the role of the SMC in this regard. The weakness of the Cadet and Nnoli (1987) study is the little attempt to relate their findings to the seasonally varying regional circulations and surface conditions. It is important to consider the mean annual cycle of the water vapour transports, making

use of available reanalyses datasets, and to consider in more detail how this relates to the regional circulations.

Although the Cadet and Nnoli (1987) study was based on a single summer, the analysis was insightful and it is somewhat surprising that relatively little follow-up-work has taken place on this topic. Fontaine et al (2003) considered the water vapour transports and associated moisture flux convergence in the WAM region, through combining NCEP/NCAR Reanalysis fields (Kalnay et al, 1996) and observed rainfall (note that they indirectly estimated the moisture flux convergences by calculating the difference between precipitation and evaporation in the model). In addition to the Gulf of Guinea and Central Africa, they also showed that the Mediterranean was a source of moisture at low-levels for West Africa. At interannual timescales the authors noted that the relative importance of zonal and meridional moisture fluxes on rainfall variability varied with latitude, with the meridional flux becoming more important at higher latitudes. Interpretation of these results is hindered by lack of a complete understanding of the mean annual cycle of water vapour transports and associated circulations – central to our study.

As background for this study it is also worth noting a few key studies concerned with the various aspects of the annual cycle of the WAM, even though they did not deal with water vapour transport directly, nor the whole annual cycle. A complete understanding of the various phases of the annual cycle is lacking but several key phases have been discussed independently in the literature. In particular, Sultan and Janicot (2000) highlighted with observations a rapid shift in the location of the peak rainfall from the

coastal region to a location inland (~10°N) around the end of June. This phase of the annual cycle is very important for the whole region, since it represents a weakening in the rainfall at the coast and the beginning of the rainy season in the Sahelian zone. Why the rainband peak apparently fails to pause around 7°N-8°N remains unclear. Okumura and Xie (2004) highlighted with observations and modeling the importance of the cold tongue development on this seasonal shift of peak rainfall although, as we will show in this paper, their results appear to be more relevant to the onset of coastal rains in Spring. Caniaux et al (2009) have recently carried out an in-depth study of the nature and causes of the cold tongue development, but again relate its development to the rapid shift at the end of June. The view that the coastal rains diminish at the same time as the inland rains start, rather than the rainband physically moving, was initially proposed by Gu and Adler (2004) who suggested that the two "regimes" are associated with different rain-producing processes. This is also somewhat consistent with the "oceanic" and "continental" regimes described by Le Barbé et al (2002).

In recent years particular research emphasis has been given to the rapid shift in the location of peak rainfall at the end of June. Based on analysis of the NCEP reanalyses and daily rainfall from raingauges over West Africa Sultan and Janicot (2003) proposed that just before the rapid shift, which they refer to as "monsoon onset", heat low dynamics are dominant over the land north of the peak rainband (at the coast). Before the rapid shift, the heat low circulation enhances convective inhibition south of the heat low in the Sahelian region via subsidence, consistent with the observed low rainfall amounts there at that time. In addition they argued that the low-level southerly branch of the heat

low SMC brings moist air polewards, making the environment polewards of the main rainband increasingly more favorable for moist convection. Once deep moist convection starts in this region, they argue that the southerly monsoon flow is enhanced due to the release of inertial instability consistent with Tomas and Webster (1997). They suggested that the timing of the rapid shift is associated with an enhancement of the heat low due to lee-troughing south-west of the topography in this region that results in a rather complicated sequence of events that clearly requires further investigation.

In addition to the analyses cited above several modeling studies have recently considered the seasonal evolution of the WAM. All have focused on the rapid change in rainband location at the end of June and all have emphasized the role played by the heat low. Sijikumar et al (2006) highlighted the importance of the heat low intensity before the shift whereas Ramel et al (2006) suggested that a rapid change in the location of the heat low, from 10^{o}-15^{o}N to 20^{o}-25^{o}N, is key. Somewhat in agreement with Sultan and Janicot (2003), Hagos and Cook (2008) suggested that the heat low is associated with marked boundary layer moisture flux convergence during May that leads to a net supply of moisture to the column and condensational heating by the end of May. They argued that the heating and associated surface pressure gradients introduce inertial instability that encourages the establishment of the main rainband inland by the end of June. These studies each emphasized a certain aspect of the WAM. We argue that the WAM can be better described and understood in the context of the continuous annual evolution of the circulation and its water vapor transport.

The major aim of this study is to explore the seasonally varying regional circulations, emphasizing the role they play in determining the water vapor transport, moisture flux convergence and associated rainfall, and including how they relate to surface thermodynamic conditions. Alongside this we aim to improve our understanding of the causes of the irregular poleward advancement of the rainband between the ocean and the land during Spring and Summer. To achieve this, the paper is organized as follows. Section 2 discusses the data and methodology. In Section 3 we will provide a brief overview of the mean annual cycle of the regional circulations to complement previous observations on the same subject. In section 4 we show and interpret the annual cycle of the regional water vapour transport, the moisture flux convergence/divergence patterns and associated rainfall. Section 5 will provide some discussion and a summary with final comments is provided in section 6.

2. Data and Methodology

The analysis presented in this paper makes extensive use of the most recent ECMWF reanalysis dataset (ERA-interim) at 1.5^{o} horizontal resolution and for the period 1989-2009 (Simmons et al, 2007, Uppala et al, 2008). It should be noted however that different reanalysis products exhibit different characteristics in the West African region (Zhang et al, 2008, Meynadier et al, 2010) and so caution is needed in focusing on the details of one analysis in isolation. Rather than showing results from all available reanalyses, the pragmatic approach taken here is to consider results based on one reanalysis dataset, highlighting the aspects of the annual evolution we have most confidence in because they are reproduced in other reanalysis datasets. For completeness, however, in the Appendix

we will compare the analysis based on ERA-interim with a similarly high resolution reanalysis from the NASA, MERRA (Rienecker et al, 2009). This comparison of reanalyses will serve to guide our confidence limits in the main results presented here and will highlight areas to be investigated in future reanalyses and field campaigns.

To provide a broad perspective of the annual cycle we will first consider analyses of seasonal means (Jan-March, April-June, July-September, October-December). More detailed analyses of the annual cycle will be viewed in the context of latitude-time evolution in key fields averaged between 10°W-10°E. Following Cadet and Nnoli (1987) we will consider the moisture fluxes in two layers: surface-850hPa which we will refer to as low-level and 850-500hPa which we will refer to as mid-level. We do not consider the moisture fluxes for layers above this since they are small (due to the low humidity) and have a negligible role in influencing the annual cycle of the WAM (c.f. Fig. 11). The moisture flux is defined by the following equation:

$$F_v = \frac{1}{T}\int_0^T -\frac{1}{g}\left(\int_{p_b}^{p_t} q\mathbf{u}dp\right)dt$$

where g is gravitational acceleration, q is specific humidity, **u** is the two-dimensional wind, p_t and p_b represent the pressure at the top and bottom of the layer concerned and T is the averaging period. In addition we will show layer mean moisture flux convergence fields:

$$Q = \frac{1}{T}\int_0^T \frac{1}{g}\left(\int_{p_b}^{p_t} \nabla . qudp\right) dt$$

As discussed in Meynadier et al (2010) it is important to be aware of the potential errors in such analyses. Several potential sources of error exist including most importantly those associated with: (i) horizontal and vertical grid resolution, (ii) misrepresentation of assimilated observations and (iii) time truncation error due to the 6 hour time resolution. To reduce the error associated with grid resolution the analysis presented in the main body of the paper is based on the ERA-Interim dataset. ERA-Interim has half the grid-length of ERA40 and has 16 pressure-levels between 500hPa and 1000hPa compared to just 7 in ERA40. Several of the peak meridional and zonal fluxes highlighted in section 4 of this paper were around 50% stronger in ERA-Interim, which is consistent with the resolution dependence discussed by Meynadier et al (2010). It should be recognized however that since the ERA40 and ERA-Interim model and analysis systems are also different, the differences may not be just due to resolution. The errors associated with data assimilation and time truncation error require a detailed comparison with independent in situ measurements (c.f. Meynadier et al, 2010) which is beyond the scope of our study. It should be stressed here, however, that while the magnitudes of moisture fluxes and their convergence is important, the most important aspects that will be emphasized here is the time evolution of the patterns and how these relate to the regional circulations. These will also have errors associated with them but since key aspects of the seasonal evolution of the WAM based on ERA-Interim, presented here, are similar to those in ERA40 (not shown) and MERRA (Appendix) we are confident that the results are robust.

Given that a major motivation of this study is to understand the annual cycle of rainfall in the WAM region we will also consider the evolution of the rainfall in each of the reanalyses. It is important to be cautious when using rainfall based on reanalyses, given the known problems associated with the representation of rainfall in models (e.g. Janowiak et al, 1998). Here our aim is to consider the relationship between the rainfall and regional circulations in a reanalysis. Through consideration of this relationship in the annual cycle and in different reanalyses we aim to improve our understanding of the likely relationships in reality. For completeness, however we will also compare the evolution of rainfall from the reanalyses with estimates for rainfall based on the Global Precipitation Climatology Project (GPCP) pentad precipitation dataset (Xie et al, 2003).

It is important to recognize that other estimated rainfall datasets exist, including the CPC Merged Analysis of Precipitation (CMAP, Xie and Arkin, 1997), and the Tropical Rainfall Measuring Mission (TRMM) 3B42 dataset (Huffman et al, 2007). In a follow up paper Nguyen et al (2010) show that there is disagreement between these rainfall estimates in the West African and tropical Atlantic region, especially over the ocean where there is a lack of in-situ rainfall data. Following Nguyen et al (2010), here we chose to use the GPCP estimates over CMAP estimates because CMAP applies algorithms over the Atlantic that are based on validation studies in the Pacific, and we chose GPCP estimates over TRMM-3B42 because of the longer time-series. As highlighted in Nguyen et al (2010) this is certainly an issue that is worthy of future study.

3. Regional Circulations and associated Low-level Thermodynamic Conditions

3.1 Seasonal Means

In this section we briefly discuss the nature of the regional circulations including their relationship with surface temperature, pressure, and rainfall in each season. The surface temperature evolution shown in Fig. 1 highlights two key players in the annual cycle of the WAM: the hot Sahara and associated heat low that develops in spring (AMJ) and is hottest in summer (JAS), and the Atlantic cold tongue that also develops in spring and is coldest in summer. Consistent with the associated large-scale pressure gradient that exists between the hot Sahara and cold Atlantic we note the presence of the southerly monsoon flow from the ocean towards the land in Spring and Summer that brings moisture-laden air onto the continent. Outside these seasons the flow from the south-east Atlantic to the continent is very weak. Instead, the West African continent is mostly influenced by dry north-easterlies, the so-called "Harmattan" winds. We should also note the establishment of a low-level onshore westerly in Summer around 20^{o}W and 10°N that is likely a response to the latent heating in the rainband over the continent and also advects moist air onto the continent (Lamb, 1983, Grodsky et al, 2003, Pu et al, 2010).

The picture described above is of course simplistic. Important complicating additions to this picture are the circulations due to latent heat release in the annually migrating rainband and sensible heating in the Saharan heat low. Figure 2 shows seasonal means of rainfall (based on GPCP). As described in the introduction, for this range of longitudes the rainfall peak remains close to the equator or just north of it between late Fall and Winter, and is only located over the West African continent in the summer. Also,

included in Fig. 2 are the winds at 700hPa to highlight two things: the mid-level northerly return flow and the African easterly jet (AEJ), both related to the heat low (Thorncroft and Blackburn, 1999). As discussed in Zhang et al (2008) the winds at this level actually penetrate the location of the mean rainband. We will discuss the role of this northerly return flow on the progression of the rainband in section 4.

Figure 3 highlights more clearly the seasonal means of the regional overturning circulations and zonal jets. The presence of two meridional overturning circulations is clearly seen in all seasons. Note that because of the strong zonal flows, neither of these is closed. Although the heat low is relatively weak in JFM (maximum surface temperatures around 303K compared to 310K in JAS), its associated SMC is robust with a mid-level return flow that crosses the equator. This suggests that the low-level southerly flow owes its existence, at least in part, to the heat low and the related meridional surface pressure gradient established between the land and the ocean at this time (see Fig. 1a). In spring the SMC again appears to extend across the equator but the situation is complicated by the presence of the deep overturning circulation associated with the coastal rainfall (cf Fig. 2b). At this time the low-level monsoonal flow is influenced by both large-scale land-ocean temperature contrasts (Fig. 1b) and the latent heating in the main rainband (Fig. 2b) as demonstrated in Hagos and Zhang (2009). The circulations associated with these two mechanisms contribute to the moisture flux convergence very differently, (see section 4). During spring, both the monsoonal westerlies and the AEJ strengthen as the regional heating patterns shift polewards (and Coriolis deflections increase). As the rainband shifts polewards further in summer, so do the monsoon westerlies, and the

upper-level tropical easterly jet is established. As in spring, we expect the low-level monsoon southerlies to be impacted by both the land-ocean surface temperature contrasts (Fig.1c) and the latent heating in the rainband (Fig.2c). In OND, all the circulations weaken substantially although the SMC is still clearly seen, consistent with a weaker rainband at these longitudes (Fig. 2d).

Since the role of the heat low SMC is an important part of this work it is also important to recognize that it would be erroneous to attribute all of the observed northerly return flow and southerly flow beneath this to the heat low associated SMC. For example, it is possible to argue that at least part of the observed northerly flow is associated with a balanced flow consistent with a large-scale pressure gradient in the north-south direction. By way of a "proof-of-concept" Fig. 7 of Thorncroft and Blackburn (1999) shows the atmospheric response to Saharan heating and clearly highlights the presence of a cross-equatorial flow. While this may not be conclusive, since there exists a weak cross-equatorial temperature gradient in the model setup, the same experiment repeated with no cross-equatorial temperature gradient still results in cross-equatorial flow (Cornforth, personal communication). Further evidence for the presence of the SMC is found in the high resolution reanalyses examined here. Both ERA-Interim (Fig. 3) and MERRA (see Fig. A3) highlight, more convincingly than in previous coarser resolution reanalyses, the presence of a shallow north-south meridional overturning circulation. The coherency of these circulations implies that at least part of the mid-level return flow and low-level cross-equatorial flow can be attributed to the heat low SMC. A more precise study of this attribution problem should be carried out but is beyond the scope of this study.

3.2 Annual Cycle

In this section we explore in more detail the continuous annual evolution of the regional circulations and related surface conditions (Fig. 4). The main aim here is to provide the background needed to understand the varying roles of the regional circulations on the moisture transport and its convergence, and to ultimately associate this evolution with the observed rainfall in section 4.

Figure 4a highlights the evolution of the surface temperature and associated 10m meridional winds. Consistent with Fig. 1 the evolution is dominated by two processes: warming of the Sahara associated with the developing heat low that begins in February and cooling of the equatorial SSTs associated with the developing cold tongue that begins in April. The warming over the continent moves polewards due to the movement of the surface solar heating and a cooling of the land surface (5 – 10˚N) by evaporation of rainfall that keeps increasing over land through the boreal spring (Fig. 4c). In contrast, maximum cooling of the ocean surface is geographically fixed just south of the equator and is driven by meridional and zonal surface wind stresses (Okumura and Xie, 2004, Caniaux et al, 2009). Note that prior to the ocean cooling in April, the equatorial region is characterized by a wide area of warm water with values greater than 28^{o}C. This whole area cools down rapidly between April and June. Associated with this cooling is a rapid rise in mean sea level pressure (MSLP) at the equator with peak values on the equator rising from 1010hPa in April to 1014hPa in June (Fig. 4b).

The temperature and related MSLP changes are associated with significant changes in the regional circulations. The surface meridional winds (Fig. 4a) highlight a region of confluence immediately south of the warmest surface temperatures over the land. This region of confluence is often referred to as the Inter Tropical Front or Discontinuity and has been the subject of several recent papers (e.g. Bou Karam et al , 2008, Lele and Lamb, 2010). South of this, the southerlies prevail across the equator throughout the year. Of particular relevance to the above discussion is the acceleration of the low-level southerlies in the equatorial region between April and June that coincides with the cold tongue development and associated MSLP rise. Cross-equatorial southerly flow doubles (from 2 ms^{-1} to 4 ms^{-1}) between April and June. Moving between summer and winter, the strength of these features weakens, the location of the warmest surface shifts southward and the equatorial region warms up again.

Another notable aspect of the annual evolution seen in Fig. 4(a) is the establishment of a prominent region of low-level convergence at the coastline (~5^{o}N) in June. This remains a prominent feature throughout the summer months and was briefly mentioned in Meynadier et al (2010). As we will show later (see section 5) this is a shallow feature that likely arises in association with frictional convergence at the coast and has received little attention in the literature.

Included in Fig. 4b and c is the wind at 700hPa. The diffluence in meridional wind at 700hPa (Fig. 4b) clearly sits above the surface confluence all the time, consistent with the presence of the SMC (Zhang et al, 2008). The return flow towards the south appears to

cross the equator between November and April, but is very weak or absent between May and October. The strengthened deep convective heating and weakened shallow convective heating in the summer months may explain the weak cross-equatorial return flow in ERA-interim (Nolan et al 2007, Zhang et al, 2008). It is interesting to note that there is no acceleration in the 700 hPa northerlies equivalent to that observed in surface southerlies between April and June, suggesting that the poleward moving surface air converges, ascends, then diverges and flows equatorward at a higher level as part of the deep overturning circulation. There is indeed an acceleration of the northerlies at 200 hPa at this time (not shown).

Figure 4c shows the mean rainfall together with wind vectors at 700hPa. Starting at the beginning of the year, the peak rainfall is located close to the equator. Between March and May the peak shifts polewards to the coastal region. This is the wettest part of the WAM seasonal cycle. Mean peak values of about 10 mm day^{-1} occur at the end of May around 4^{o}N (over the ocean). Between June and July there is a weakening in the peak rainfall totals and following this a relocation of the peak rainfall to about 10^{o}N. After August the peak rainfall moves back towards the ocean relatively smoothly. The peak easterlies generally lie just poleward of the rainfall peak, consistent with the idea that potential vorticity generated by the deep moist convection acts to maintain the AEJ (see Schubert et al, 1991, Thorncroft and Blackburn, 1999). The northerly component of the wind can also clearly be seen with the winds blowing through the latitude of the rainband towards the equator. Notice however that the northerly component tends not to be seen on the equatorward side of the rainfall in ERA-interim, except in the periods of weaker

rainfall during winter months. This suggests that in periods of strong rainfall, on reaching the latitude of peak rainfall, the SMC return flow generally ascends into the deep convecting region (cf Fig. 3).

For completeness Fig. 5 shows the annual evolution of the low-level equivalent potential temperature, θ_e. Following Emanuel (1995) and Zheng et al (1999) the deep tropospheric direct circulation associated with north-south variations in rainfall is expected to be related to the distribution of low-level gradients in θ_e. with the peak in rainfall preferentially occurring in the region of highest θ_e. As shown in Fig. 5, the location of the peak in low-level θ_e moves between a location just north of the equator in January to its most poleward location of 15^{o}N in July and August. The highest θ_e values are reached between April and May when they are located between about 7-10^{o}N, over land. The fact that the highest values are peaked over the land then is associated with the high absolute humidity values there combined with high surface temperatures (that peak poleward of this). Comparing this evolution with the location of peak rainfall included in Fig. 5 (as defined by GPCP) we note that peak rainfall is always equatorward of the peak θ_e, especially during spring and summer when the peak θ_e is over the land. We suggest that this is associated with the fact that the regions of highest θ_e over the land are overlain by warm (and dry) Saharan air (compared to the region south of this). The relatively higher convective inhibition there is therefore consistent with the preferred location for peak rainfall south of this (Parker et al 2005). We argue that while the north-south contrasts in θ_e are important for driving the direct overturning circulation, consistent with Emanuel (1995), the peak in θ_e, especially when over the continent, is a very poor indicator of

where the peak in moist convection is. This, of course, is due to the role of the heat low and the stabilizing effect of its associated SMC.

4. Water Vapour Transport and Moisture Flux Convergence

4.1 Seasonal Mean Moisture Fluxes

Here we provide a brief overview of seasonal mean moisture transport for each season. This extends the analysis of Cadet and Nnoli (1987) who only considered a single year and just the May-September period. It also provides the 3-dimensional context for the following sections which are based on zonal averaged fields between 10^{o}W and 10^{o}E. Following Cadet and Nnoli (1987) we consider the vertically integrated moisture flux between the 1000-850hPa (the approximate depth of the monsoon layer) and between 850-500hPa to highlight the moisture transport at mid-levels. We also consider the meridional and zonal fluxes separately.

Figure 6 shows the seasonal means of the meridional moisture flux at low-levels together with the location of the peak rainfall as seen in the GPCP and ERA-interim datasets. Consistent with the low-level winds presented in Fig. 1, the eastern equatorial Atlantic is characterized by a southerly moisture flux penetrating through the location of the mean rainband peak all year long (Fig. 2). Indeed, there is an on-shore moisture flux, in the Guinea Coast region, throughout the year consistent with the fact that the MSLP minimum in the West African region is always located over the land (Fig. 1). The peak southerly flux is in Spring (AMJ) with values of about 90 $kgm^{-1}s^{-1}$ located close to the equator. The southerly flux is weaker in the other seasons with values in the $70kgm^{-1}s^{-1}$

range. The poleward extent of the southerly moisture flux increases during Spring and reaches its most northern latitude around 20°N, close to the center of the heat low, in Summer (JAS). Indeed, the poleward extension of the southerly flux is directly determined by the location of the heat low in all seasons (Fig. 1).

The zonal moisture fluxes at low-levels also exhibit marked seasonality (Fig. 7). Consistent with the mean easterly trade winds, much of the Atlantic is characterized by easterly fluxes with values greater than 150 $kgm^{-1}s^{-1}$ in the central Atlantic in all seasons. Perhaps more relevant to the WAM is the establishment of westerly fluxes onshore and over the West African continent. Over the West African continent the highest values occur in Spring and Summer with highest values around 90 $kgm^{-1}s^{-1}$. The poleward extent of the westerly flux over the continent appears again to be determined by the location of the heat low (Fig 1). Over the ocean the highest values occur in Summer in two regions: just west of the Cameroon highlands (around 5°E, 5°N) where the peak is around 90 $kgm^{-1}s^{-1}$ and just west of the Guinea highlands where the peak is about 60 $kgm^{-1}s^{-1}$.

The seasonal mean of the meridional moisture flux at mid-levels is shown in Fig. 8. A combination of low humidity and low meridional wind speed results in much lower moisture fluxes compared to those at low levels. Northerly moisture fluxes are seen over the eastern equatorial Atlantic throughout the year. These peak over West Africa in Spring when the values reach up to -50 $kgm^{-1}s^{-1}$. In contrast, the zonal moisture fluxes at mid-levels are large with peaks greater than those seen at low-levels (Fig. 9). The WAM region is dominated by easterly moisture fluxes consistent with the presence of the AEJ.

Values peak in Spring and Summer when they reach about -170 $kgm^{-1}s^{-1}$. It should be noted however that at low-levels and mid-levels in the region defined by 10^{o}W to 10^{o}E, the zonal flux into and out of the region is approximately equal resulting in little contribution to the regional moisture flux convergence.

4.2 Annual Cycle of Moisture Flux Convergence and associated Moisture Fluxes

Figure 10 provides detailed information about the annual variations of daily moisture fluxes and their associated convergence, including a breakdown of the contributions from low and mid-levels. Also included in this figure are the low and mid-level moisture fluxes in the meridional direction. The fluxes in the zonal direction are not included since they do not significantly contribute to the moisture flux convergence for this range of longitudes (Fig. 7 and 9). Figure 10a shows the total column moisture flux convergence together with the position of the heat low (defined by the latitude of the potential temperature maxima at 925hPa over the continent), and rainfall maxima. A broad migrating latitudinal band of moisture flux convergence exists between the equatorial region and around 20^{o}N, roughly coincident with the observed rainfall (Fig. 4c). A similarly broad region of moisture flux divergence is present equatorwards of this consistent with the subsiding branch of the deep overturning circulation, and is strongest in spring, consistent with the highest rainfall rates at that time of year.

In fall and winter (approximately between October and February), the moisture flux convergence occurs in a narrow band (~6^{o}) that peaks close to the equator. In spring and summer (February – September) a second region of weak moisture flux convergence is

established just south of the heat low centre suggesting a role for the heat low SMC. Weak moisture flux divergence also generally characterizes the region between the two peaks that is also likely associated with the intensifying heat low. Within this broad region of moisture flux convergence that affects about 18^{o} of latitude, the highest values (indicated by shading) are always on the equatorward side. Their location and timing are roughly coincident with those of the peak rainfall and associated deep latent heating (Schubert et al, 1991, Hagos and Zhang, 2009). Note, however, that the peak in moisture flux convergence is a few degrees of latitude equatorward of the peak in GPCP rainfall between June and August consistent with a dry bias of the ERA-interim model in summer, a previously documented characteristic of the ECMWF model (Agusti-Panareda et al, 2010, Meynadier et al, 2010, see also Fig 6c).

Figures 10b and c show the contributions to the column moisture flux convergence from low-levels (1000-850hPa) and mid-levels (850-500hPa) which can in turn be interpreted by comparing with the meridional flux component in Figs. 10d and e. The low-level moisture flux convergence has peak values always north of the rainfall peak, just south of the heat low centre. While most intense in spring, this is a prominent feature throughout the year. A much weaker region of moisture flux convergence is approximately collocated with the peak of the rainband. Notably, however, the rainfall peak lies a few degrees poleward of the moisture flux convergence in summer (JAS), at a time when the low-level meridional wind is strongly convergent at the coastline (cf Fig. 4a). The rainfall in summer is actually collocated with the moisture flux convergence at mid-levels (Fig.

10(c)). This structure will be seen more clearly in vertical cross-sections that will be discussed in section 5 below.

We should note that a band of marked moisture flux divergence at mid-levels offsets the northern convergence maximum at the low levels, resulting in the relatively weak total column moisture flux convergence in Fig. 10a. This pattern of low-level moisture flux convergence overlain by mid-level moisture flux divergence is clearly associated with the heat low SMC and was also recently noted in the modeling results of Hagos and Cook (2008)[1]. The role of the SMC in this can be seen clearly in the low and mid-level meridional fluxes (Fig. 10d and e). At low-levels the location of zero meridional flux follows the heat low center and is flanked by northerly flux to the north and much stronger southerly flux to the south. At mid-levels the opposite pattern can be seen. The fact that the low-level moisture convergence peaks equatorward of the heat low center is consistent with previously described dry dynamics (see Thorncroft and Blackburn, 1999) together with the higher values of moisture there. Also, the net positive moisture flux convergence in the column arises due to the larger moisture values at low-levels compared to mid-levels and is associated with a moistening of the column that is particularly marked between February and May (not shown).

5. Discussion

We now discuss and interpret in more detail the evolution of the West African monsoon focusing in particular on four phases of the poleward progression of the peak in moisture

[1] There is a similar cancellation between low-level and mid-level moisture flux convergence and divergence respectively in the Mediterranean coastal region between 30°N and 35°N between April and October.

flux convergence and the associated rainfall. The motivation for defining these phases comes from Figs. 4c and 10a which clearly highlight two distinctive periods of elevated rainfall and moisture flux convergence associated with the main rainy season at the coast between about mid-April and the end of June (*Coastal phase*) and the rainy season in the Sahel between mid-July and September (*Sahelian phase*). The other two phases are: a period when the moisture flux convergence peak and associated rainfall are close to the equator between November and mid-April (*Oceanic phase*), and a period between the end of the coastal phase and the beginning of the Sahelian phase (*Transitional phase).* The transitional phase is characterized by rainfall that is weaker than in both the coastal and Sahelian phases, and it occurs during the first half of July. During this period the location of the peak GPCP rainfall moves from its position close to the coast to the Sahel. To support the discussion of the different phases Fig. 11 shows north-south vertical cross-sections of moisture flux convergence for the four phases together with vertical-meridional wind vectors.

(a) Oceanic phase (November to Mid-April)

The oceanic phase corresponds to the period of warmest SSTs in the tropical Atlantic and a time when peaks in low-level θ_e and θ are approximately collocated over the ocean (Figs. 4a and 5), although they start to be displaced at the end of this phase. The vertical cross-section of moisture flux convergence averaged for this period highlights the features discussed in the previous section (Fig. 11(a)). The vertical dipole structure associated with the heat low SMC is clearly visible at this time around 10^{o}N. There is also a weak moisture flux convergence peak located around 700hPa and 5^{o}S which, we

suggest, is linked to the SMC return flow (Fig. 3(a)). The low-level moisture flux divergence in the southern hemisphere associated with the large-scale cross-equatorial flow is also prominent. At the latitude of the peak rainfall (~1^{o}N) the column moisture flux convergence is clearly positive with the largest contribution coming from low-levels, below about 900hPa.

(b) Coastal Phase (Mid-April to June)

Between April and May the peak in column moisture flux convergence increases and moves polewards from its winter location close to the equator to the coast (~4^{o}N), where it remains collocated with the warmest SSTs. This northward shift is coincident with the development of the cold tongue, the associated rise in MSLP and acceleration of the southerly wind at low-levels discussed above (Fig. 4). The peak in May is significant because it coincides with one of the wettest months of the year for the WAM and the shift is significant because it coincides with the rapid intensification of the rains for the coastal countries that are just north of the peak in rainfall (Figs. 2(b) and 4(c)). The peak in column moisture flux convergence is again dominated by low-levels with a weaker contribution at mid-levels (Fig. 11b). The low-level peak in moisture flux convergence is associated with a strengthening of the southerly flux south of the equator (cf Fig. 10(d), Fig 6(b)), that is enhanced during the cold-tongue development in Spring. The fact that the southerly flux peaks in Spring and not in Summer when the meridional winds are slightly stronger (Fig. 4(a)) is due to the moister low-levels in Spring which in turn is consistent with the warmer SSTs just prior to the cold tongue development. The low-level

layer averaged specific humidity in the equatorial region decreases from about 15.5gKg^{-1} in April to about 11.5gKg^{-1} in July (not shown).

One mechanism that appears to be operating is one that was originally proposed by Zheng et al (1999) to interpret anomalously wet years in the Sahel. Warm SSTs in the Spring are associated with a relatively moist boundary layer. Once the cold tongue starts to develop, the rapid cooling is associated with a rapid rise in surface pressure. The meridional pressure gradient results in an acceleration of the low-level southerlies and large poleward moisture fluxes towards the continent. While the southerlies may intensify after this, consistent with the continued development of the cold tongue, the cold SSTs will be associated with a drier boundary layer compared to the Spring. We suggest that this mechanism could be a fundamental component of the mean annual cycle and is particularly relevant to the high rainfall close to the coast around May.

An additional mechanism that is likely operating in concert with this involves the SMC associated with the heat low. As highlighted by Zhang et al (2008), and also shown in Fig. 3b, the fact that the mid-level return-flow emanating out of the heat low region crosses the equator suggests that the low-level southerlies are related to the heat low SMC. It is difficult to quantify the relative roles of the cold tongue and the heat low on the timing and strength of the cross-equatorial southerlies from these analyses since the acceleration occurs at a time when both the cold tongue and heat low are rapidly intensifying (Fig. 4a). However, the fact that the heat low clearly starts to intensify in

February, before the cold tongue development, suggests that the heat low SMC may well influence the cross-equatorial southerlies first.

A characteristic feature of the moisture flux convergence pattern during April and May is the presence of a significant region of mid-level moisture flux convergence just poleward of the peak in rainfall (Figs. 10c and 11b). This peak, which was south of the rainfall peak during the oceanic phase, is connected to the low-level peak of the heat low, now forming a continuous upward-equatorward tilt of the convergence zone. As mentioned above, a key aspect of this appears to be the equatorward moisture flux associated with the return flow of the SMC (Fig. 10e). This suggests a rather intriguing situation – while the return flow is associated with advection of relatively warm and dry air equatorwards (not shown) that has a negative impact on moist convection through stabilizing the thermodynamic profile, equatorward of this, the return flow is associated with moisture flux convergence which likely has a positive impact on moist convection there. Thus the mid-level return flow appears to favour a southern location for the rainband. In contrast, the low-level moist southerlies beneath this are associated with marked moisture flux convergence poleward of the peak in rainfall and, through low-level moistening (not shown), appears to favour a northern location for the rainband. The relative importance of these processes may change during the evolution of the WAM and may influence the intensity of the peak in the rainband.

Another notable feature in Fig. 11b is the separation of low-level coastal and heat-low moisture convergence with low-level moisture flux divergence in between. This appears

to be another characteristic of the heat low associated SMC. As the heat low moves northward, the coastal convergence remains at roughly the same location. Indeed we believe that the prominent quadrapole structure in the moisture flux convergence on the poleward side of the rainfall peak is mostly, if not all, related to the presence of the heat low SMC and clearly has a dominant role on the moisture flux profiles there.

By the end of this phase the rainfall peak and the associated column total moisture flux convergence peak have weakened and shifted from the ocean onto the continent (cf Figs 10a and A-1ab,). Also, as already noted in section 3.2, by the end of this phase a prominent region of low-level convergence is established at the coastline that remains in this location until the end of summer (Figs 11b,c,d). Given its location we argue that this peak in convergence arises in association with a deceleration of the low-level wind as the air moves between the ocean and the continent. This feature has not received much attention in the literature and its prominence now is likely linked to the higher vertical resolution of the ERA-interim reanalyses, with 5 pressure levels between 900hPa and the surface, compared to ERA40 (for example) which only had two. It is possible that, in addition to the warm SSTs close to the coast, the frictionally-induced low-level moisture flux convergence at the coast could be an additional factor that encourages the peak in rainfall to persist close to the coast rather than move more steadily into the continent (analogous to its retreat between September and October).

(c) Transitional Phase (1-15 July)

During the first half of July the ERA-interim rainfall peak (and the associated total column moisture flux convergence) in the coastal region continues to weaken and moves a little further inland (Fig. A1b, Fig. 10a). The simplest explanation for the reduction in coastal rainfall relates to the cooling of the SSTs close to the coast (Fig. 4a). Between April and June the SSTs around 5^{o}N drop below 28^{o}C, a threshold known to be important in this region (Nguyen et al, 2010). This cooling is likely due to a combination of processes: an expansion of the developing cold tongue, and local wind-driven coastal upwelling, possibly including that associated with coastal Kelvin waves propagating from the equatorial region (Polo et al, 2008).

The moisture flux convergence structure during this phase looks very similar to that during the coastal phase, with a peak in low-level moisture flux convergence close to the coast where the peak rainfall is and, polewards of this, the prominent quadrapole structure consistent with the heat low associated SMC. Figure 11c also highlights the establishment of a north-south moisture flux convergence-divergence dipole, around 850hPa and centered near 7.5^{o}N, that was only hinted at in the coastal phase. The southern moisture flux divergence peak around 4^{o}N contributes to the weaker column total at this time while the northern moisture flux convergence peak around 10^{o}N increases the column total there. The associated poleward flow that peaks around 850hPa is likely a response to latent heating around 10^{o}N with peak heating above this level. The fact that this dipole structure intensifies in the Sahelian rainfall phase is consistent with this (Fig. 11d).

(d) Sahelian Rainfall Phase (mid-July-September)

Figure 10a indicates that during July the location of the peak moisture flux convergence shifts from about 7°N to about 10°N and strengthens, consistent with the onset of the rainy season in the Sahel (Fig. 4c). Previous studies of the rainfall onset in the Sahel have emphasized the abrupt shift in the location of peak rainfall from around 5°N to 10°N between June and July (Sultan and Janicot, 2003; Hagos and Cook, 2008; Gu and Adler, 2004). Viewed in terms of the location of peak moisture flux convergence the transition appears to be less dramatic with the change in latitude taking place fairly steadily between June and July (note the steady poleward movement of the zero contour in Fig. 10a). From this perspective, an important characteristic of the monsoon that requires explanation is the reduction in coastal rainfall and associated moisture flux convergence during the transitional period.

The vertical structure of moisture flux convergence in the Sahelian phase is very similar to that in the transitional phase except for a slight intensification of the north-south dipole structure at 850hPa. This suggests that the Transitional and Sahelian phases do not represent periods characterized by fundamentally different physics. It does suggest however that the processes responsible for weak convection in the Transitional phase are overcome somewhat in the Sahelian phase. One possibility is that MCSs become more favorable at this time due to the combination of increased conditional instability (linked to low-level moistening by the heat low SMC) and increased topographic triggering of convection.

The vertical structure of moisture flux convergence near the peak rainfall in the Sahel is complicated and characterized by three peaks: (i) the coastal low-level peak that remains prominent (likely to be frictionally induced as discussed above), even though the rainfall peak moved away inland, (ii) a weak peak at 850hPa that is likely linked to a latent heating maxima above that level in the Sahelian region (e.g. Schumacher et al, 2004)) and (iii) another weak peak at 750hPa that is linked to the SMC return flow. The equatorward tilt of the convergence zone from low to mid levels does not exist any more. It remains a challenge to understand this rich structure and how it combines to influence the nature of the rainfall. In addition, it certainly remains a challenge for dynamical models to represent it (c.f. Meynedier et al, 2010).

6. Summary and Concluding Remarks

The major aims of this paper are to explore the nature of the seasonally varying regional circulations including their relationship to surface conditions and water vapor transport in the West African region and, thereby, to increase our understanding of the irregular poleward movement of the main monsoon rainband. The analysis, aided by the recently available higher resolution ERA-Interim and MERRA reanalysis datasets (see Appendix), has made progress towards addressing these aims. Perhaps most importantly, this analysis provides new perspectives on the evolution of the WAM rainfall from winter to summer in terms of four phases summarized in section 5 (and below). Also, by focusing on the seasonal evolution of the moisture flux convergence we have been able to provide new insight on the irregular poleward movement, especially regarding the coastal onset in spring.

The annual evolution of the moisture fluxes, their convergence, and associated rainfall is strongly affected by the Atlantic equatorial cold tongue and Saharan heat low. The cold tongue strongly regulates the timing and intensity of the coastal rainfall in spring. The heat low and its associated SMC strongly affect the profile in moisture flux convergence north of the main rainband maximum throughout the year; in particular it is responsible for the establishment of a second peak in total column moisture flux convergence there. While we believe that the pattern of SMC-associated moisture flux convergence is robust, as highlighted in Meynadier et al, 2010, its amplitude may be exaggerated in ERA-Interim fields and so this aspect of the SMC should be explored in more detail in future studies. In addition, this study has highlighted a new and prominent coastal moisture flux convergence that we believe is frictionally induced and is a feature that persists between spring and summer. We hypothesize that, in addition to warm SSTs, this coastal moisture flux convergence may have a role in delaying the movement of the rainband inland.

This study describes the progression of the West African monsoon in the region between 10^{o}W and 10^{o}E in terms of four key phases. Each phase is summarized here and in the schematic included in Fig. 12.

(i) Oceanic phase (November to mid-April):

The main rainband, and associated column moisture flux convergence, is broad with peak values close to the equator, where SSTs are warmer than 28^{o}C over a wide area. Little rain falls over the West African continent in this phase. As the heat low

intensifies between February and March the area of column moisture flux convergence broadens and extends poleward consistent with the increased importance of the heat low associated SMC. By the end of this phase, SSTs in a broad longitudinal range close to the equator start to fall, which marks the development of the cold tongue and initiation of the annual northward migration of the rainband. The SMC associated with the intensifying heat low in February may contribute to a cross-equatorial flow that leads to the cold tongue development but this is clearly an area that needs further study. At the latitude of the peak rainfall the moisture flux convergence profile is characterized by a major peak at low-levels and a minor peak at mid-levels that is likely associated with the return flow of the heat low SMC.

(ii) Coastal phase (mid-April to end of June):

Between April and May equatorial SSTs drop below 28^{o}C and the peak in rainfall moves from there to the coastal region around 4^{o}N where SSTs remain greater than 28^{o}C. This is the wettest phase of the annual cycle. A key aspect of the coastal onset in May is the acceleration of low-level cross-equatorial southerly winds, important for establishing the cold tongue as well as transporting moisture towards the coast. Both the cold tongue development itself and the heat low are likely contributing to the acceleration at this time but their relative importance needs to be quantified. By the end of this phase, while the peak in rainfall shifts in land and the heat-low convergence moves northward, the coastal moisture flux convergence appears to be enhanced due to frictional deceleration of the low-level winds over land. During the coastal phase a marked quadrapole structure in moisture flux convergence becomes

established on the poleward side of the peak in rainfall (highlighted with red contours in Fig. 12b) consistent with the presence of the heat low SMC. It is possible that a similar quadrapole structure is present in the oceanic phase with its southern part located close to the equator but other features in the moisture flux convergence field prohibit us making stronger statements in this regard. Once established, both the low-level moisture flux convergence at the coast and the heat low associated quadrapole structure poleward of the peak in rainfall are maintained throughout the summer.

(iii) Transitional phase (First half of July):

At the end of June the coastal peak rainfall decreases markedly while the coastal moisture flux convergence remains strong. The fact that the peak rainfall weakens at the end of June enhances the perception that the rainband rapidly shifts between the coastal region and the Sahel at the beginning of July (cf Fig. 4(c)). The column moisture flux convergence moves poleward more gradually than implied by previous studies. The reduction in the peak rainfall is consistent with lower SSTs in the coastal region as well as stabilization by advection of warm dry air by the return flow of the heat low SMC north of this (cf Sultan and Janicot, 2003). During this phase a moisture flux convergence-divergence dipole becomes established around 850hPa and centered near 7.5^{o}N (highlighted with green contours in Fig. 12(c)). We hypothesize that this arises in part as a response to latent heating in the Sahelian region but, again, this should be investigated further alongside available observations.

(iv) Sahelian phase (mid-July-September):

By mid-July the peak in the rainfall intensifies and becomes established in the Sahelian region around 10°N. The moisture flux convergence profile near the peak rainfall has three main peaks: (i) the low-level peak centered at the coast, (ii) the peak around 850hPa perhaps linked to latent heating (as discussed above) and (iii) the mid-level peak linked to the return flow of the heat low SMC and perhaps also to upper-level latent heat release. The relative importance of these peaks including their influence on the behavior of the convection and associated rainfall should be investigated in more detail alongside available observations.

A major recommendation motivated by this work is the need to consider in more detail the nature of the coastal rainfall including its onset and subsequent weakening prior to the establishment of inland rainfall peak (July and August). It is surprising that, given its intensity and especially its significance to the populations living in the coastal region, the coastal rainfall phase has not received more attention in the literature. The West African Monsoon clearly experiences two significant rainfall onsets, one at the coast, and a second inland. The results presented here suggest that the cold tongue development and the heat low SMC are both key components of the monsoon evolution. The cold tongue development is key for the timing of the coastal rainfall onset. The heat low SMC is also certainly instrumental to the poleward rainfall migration throughout the February to July period.

Previous studies concerned mainly with the Sahelian rainfall onset have given strong emphasis to the role played by inertial instability at low-levels in determining the rapid change in the location of peak rainfall at the beginning of July (e.g. Sultan and Janicot (2003), Hagos and Cook (2008), Nicholson and Webster (2007)). As discussed above, our analysis of the moisture flux convergence suggests that the rapid change in the location of the rainfall appears to occur in a slowly evolving large-scale environment and can be investigated in terms of the weakening of the coastal rainfall peak at the end of June and intensification of Sahelian rainfall in July. This suggests that more emphasis should also be given to variations in stability of the atmosphere to convection and, given the important role of mesoscale convection to the Sahel, whether the environment becomes more favorable for triggering of mesoscale convective systems (e.g. Laing et al, 2008).

Three areas of the WAM evolution require further detailed study. First, more work is required to elucidate the processes that determine the nature of the cold tongue development including especially the time when the cooling begins (Nguyen et al, 2010). Our results hint at the possibly important role played by the heat low SMC in the February to April period but more detailed analysis of available observations and possibly some modeling are needed. This should include much-needed in situ measurements of the atmosphere and ocean in the tropical Atlantic. Second, future work should consider, in more detail than was possible here, the nature and role of the coastal maximum in moisture flux convergence that persists between late Spring and Summer. The extent to which this feature has a role in the persistence of the coastal rainfall should

be explored. Finally, more work is needed on the evolution of the vertical moisture profiles associated with the rich structure of moisture flux convergence highlighted here. This should include how this impacts stability of the atmosphere in order to shed more light on the evolution and intensity of the rainfall peak in all phases. The impact of the heat low SMC on these profiles deserves particular attention.

APPENDIX

Comparison of Reanalyses

Given the known differences in how the regional circulations in the West African region are represented in different reanalyses (e.g. Zhang et al, 2008), it is important to compare the analysis presented in this paper using ERA-Interim with other high resolution reanalysis datasets. Key diagnostics have therefore been repeated with another high resolution reanalysis dataset created by NASA (MERRA, Rienecker et al, 2009) which has a horizontal grid length of 1.125^{o} (compared to 1.5^{o} for ERA-Interim) and has 17 pressure levels between 1000hPa and 500hPa (compared to 16 levels for ERA-Interim). Characteristics that both reanalyses share can be viewed with greater confidence than those that are not. Areas of disagreement suggest reduced confidence and should motivate exploration of observations independent of the reanalyses. To aid the discussion, Fig. A.1 shows the annual cycle of rainfall from the two reanalyses together with that from GPCP. While it is recognized that the modeled rainfall should be viewed with caution, the differences between the reanalyses will help interpret the comparison here.

The MERRA rainfall has characteristics that are broadly similar to that produced by the ERA-Interim (Fig. A.1b,c). Both reanalyses have a well-defined *oceanic phase* in winter and early spring when rainfall is present over a broad latitudinal range with peaks over the ocean and low rainfall in the coastal region. Both reanalyses are notably wetter over the ocean than GPCP suggesting the need for more observations to evaluate the models as well as the rainfall estimate (cf Nguyen et al, 2010). As in ERA-Interim and GPCP, MERRA has a well-defined *coastal phase* with peaks in rainfall just south of the West African coastline in April and May. MERRA is also characterized by a weakening of the peak rainfall in the *transitional phase* although peak values are higher than in ERA-Interim and GPCP. This suggests that the processes that suppress rainfall in this phase in the ECMWF model, and possibly in reality, are not so dominant in the MERRA model. As with ERA-Interim, the rainfall in MERRA during the Sahelian phase does not penetrate as far north as that estimated in GPCP highlighting a similar dry bias in the Sahel during summer (see Agusti-Panareda et al, 2010, Meynadier et al, 2010).

Figure A.3 shows the seasonal mean regional circulations and potential temperature using MERRA for comparison with the same fields in ERA-Interim (Fig. 3). It is important to notice that the key features of the regional circulations are reproduced in the MERRA analysis. Most importantly this includes a marked SMC in all seasons with characteristic ascent in the lower troposphere on the warm side of the low-level baroclinic zone and a northerly return flow around 700hPa that coincides with the peak in easterly winds over the continent. As in ERA-Interim, the coherent structure suggests that the heat low associated SMC contributes to the strength of the low-level southerly flow, especially in

winter and spring. While the consistency between the two reanalyses regarding the nature of the SMC is encouraging one should still be cautious about the fidelity of the reanalyses with respect to how they represent its strength. Meynadier et al (2010) suggest that in several of the reanalyses they considered (including ERA-Interim) it is too strong poleward of the main rainband and that this is consistent with anomalous column moisture flux divergence around 13-16^{o}N. This itself is consistent with the well known dry precipitation bias in the ECMWF model (e.g. Agusti-Panareda et al, 2010), an issue that should be explored in more detail in future studies.

For a more detailed comparison of the reanalyses we reproduce Fig. 10 with MERRA (Fig. A3). Most of the key features seen in ERA-Interim, and discussed in section 4, can be seen here. Most importantly this includes: (i) the establishment of the peak in moisture flux convergence in spring (Fig. A3a) consistent with the increased poleward moisture flux at low levels (Fig. A3b), (ii) the weaker moisture flux convergence in the transitional phase, and (iii) the enhanced moisture flux convergence at low-levels close to the coastline in summer. The most striking difference occurs during the summer. Between about 15-20^{o}N MERRA is characterized by total column moisture flux divergence (Fig.A3a) consistent with a reduction in the SMC-associated moisture flux convergence at low-levels that occurs between spring and summer (Fig. A-3b). In ERA-Interim this region is characterized by weak total column moisture flux convergence consistent with the persistent dominance of low-level moisture flux convergence over mid-level moisture flux divergence (Fig. 10bc). Given the very similar rainfall amounts in ERA-Interim and

MERRA for this range of latitudes, the consequences of this difference appear to be minimal, but nevertheless should be considered in future work.

Figure A-4 reproduces Fig.11 with MERRA. Broadly speaking, the pattern of moisture flux convergence and divergence and associated wind vectors are similar. The large-scale moisture flux divergence over the ocean is reproduced. Also the SMC-associated quadrapole structure with low-level moisture flux convergence overlaid by moisture flux divergence just south of the heat low centre and the opposite pattern south of this is also seen during and after the *coastal phase* (although the low-level moisture flux divergence is notably weaker in MERRA). At smaller scales, the low-level moisture flux convergence at the coast is also evident in all periods, although it appears to be located slightly further inland compared to ERA-Interim during the *Sahelian phase*. The dipole structure in moisture flux convergence seen around 850hPa in ERA-Interim, especially during the *transitional* and *Sahelian phases*, is hinted at in MERRA but is not as prominent. The fact that such small-scale features are represented in both reanalyses gives us confidence that they represent a real feature of the WAM. However, the extent to which the differences in the way these features are represented in the reanalyses are significant or not should be explored in future work.

References

Agusti-Panareda, A., Beljaars, A., Cardinalli, C., Genkova, I. and Thorncroft, C. 2010: Impact of assimilating AMMA soundings on ECMWF analyses and forecasts, Weath. and Forecasting, in press.

Bou Karam, D., Flamant, C., Knippertz, P., Reitebuch, O., Pelon, J., Chong, M. and Dabas, A. 2008: Dust emissions over the Sahel associated with the West African monsoon intertropical discontinuity region: A representative case-study, *Quart. J. Roy. Meteorol. Soc.*, **134**, 621-634.

Cadet, D.L. and N.O. Nnoli, 1987: Water Vapour Transport over Africa and the Tropical Atlantic Ocean During Summer 1979. *Quart. Joy. Meteorol. Soc.*, **113**, 581-602.

Caniaux, G., H. Giordani, J.L. Redelsperger, F. Guichard, E. Key and M. Wade, 2009: Coupling between the Atlantic Cold Tongue and the African monsoon in boreal and Spring and Summer. *J. Clim.*, submitted.

Chou, C., J. D. Neelin and H. Su, 2001: Ocean-land-atmosphere feedbacks in an idealized monsoon. *Quart. J. Roy. Meteorol. Soc.*, **127**, 1869-1891.

Cook, K.H. and E.K. Vizy, 2006: Coupled Model Simulations of the West African monsoon system: Twentieth and Twenty-First-Century Simulations. *J. Clim.*, **19**, 3681-3703.

Eltahir, E.A.B. and C. Gong, 1997: Dynamics of Wet and Dry Years in West Africa. *J. Clim.*, **9**, 1030-1042.

Emanuel, K.A. 1995: On Thermally Direct Circulations in Moist Atmospheres. *J. Atmos. Sci.*, **52**, 1529-1534.

Fontaine, B., P. Roucou and S. Trzaska, 2003: Atmospheric water cycle and moisture fluxes in the West African monsoon: mean annual cycles and relationship using NCEP/NCAR reanalysis. *Geophys, Res. Lett.*, **30**(3), 1117, doi:10.1029/2002GL015834.

Grodsky, S.A., Carton, J.A. and Nigam, S., 2003: Near surface westerly wind jet in the Atlantic ITCZ, Geophys. Res. Letts., 30(19), 2009, doi:10.1029/2003GL017867.

Gu, G. and R.F. Adler, 2004: Seasonal Evolution and Variability Associated with the West African Monsoon System. *J. Clim.*, **17**, 3364-3377.

Hagos. S.M. and K.H. Cook, 2007: Dynamics of the West African Monsoon Jump. *J. Clim.*, **20**, 5264-5284.

Hagos, S.M. and C. Zhang, 2009: Diabatic Heating, Divergent Circulation and Moisture Transport in The African Monsoon System. *Quart. J. Roy. Met. Soc.*, submitted.

Hodges, K.I., B.J. Hoskins, J. Boyle and C.D. Thorncroft, 2003: A Comparison of Recent Reanalysis Datasets Using Objective Feature Tracking; Storm Tracks and Tropical Easterly Waves. *Mon. Wea. Rev.*, **131**, 2012-2037.

Hoskins, B.J. and M.J. Rodwell, 1995: A Model of the Asian Summer Monsoon. Part I: The Global scale. *J. Atmos. Sci.*, **52**, 1329-1340.

Huffman, G.J., Bolvin, D. T. , Nelkin, E.J. and Wolff, D.B. 2007: The TRMM Multisatellite Precipitation Analysis (TMPA): Quasi-Global, Multiyear, Combined-Sensor Precipitation Estimates at Fine Scales, J. Hydromet. 2007; 8: 38-55

Kalnay, E., M. Kanamitsu, R. Kistler, W. Collins, D. Deaven, L. Gandin, M. Iredell, S. Saha, G. White, J. Woollen, Y. Zhu, A. Leetmaa, R. Reynolds, M. Chelliah, W. Ebisuzaki, W. Higgins, J. Janowiak, K. Mo, C. Ropelewski, J. Wang, R. Jenne, and D. Joseph, 1996: The NCEP/NCAR 40-Year Reanalysis Project. *Bull. Amer. Meteor. Soc.*, **77**, 437–471.

LeBarbe, L., T. Lebel, D. Tapsoba, 2002: Rainfall Variability in West Africa during the Years 1950-90. *J. Clim.*, **15**, 187-202.

Lamb, P.J. 1983: West African water vapor variations between recent contrasting subsaharan rainy seasons. *Tellus*, **A35**, 198-212.

Lele, M.I. and P. J. Lamb, 2010: Variability of the InterTropical Front (ITF) and Rainfall over West African Soudano-Sahel. J. Climate (in press).

Li, T., and S.G.H. Philander, 1997: On the Seasonal Cycle of the Equatorial Atlantic Ocean. *J. Climate*, **10**, 813–817.

Janowiak, J.E., A. Gruber, C.R. Kondragunta, R.E. Livezey, and G.J. Huffman, 1998: A Comparison of the NCEP–NCAR Reanalysis Precipitation and the GPCP Rain Gauge–Satellite Combined Dataset with Observational Error Considerations. *J. Climate*, **11**, 2960–2979.

Kalnay, E., and Coauthors, 1996: The NCEP/NCAR 40-Year Reanalysis Project. *Bull. Amer. Meteor. Soc.,***77,** 437–471.

Laing, A.G., R. Carbone, V. Levizzani, and J. Tuttle, 2008: The propagation and diurnal cycles of deep convection in northern tropical Africa. *Quart. J. Roy. Meteor. Soc.*, **134**, 93–109.

Meynadier, R., O. Bock, S. Gervois, F. Guichard, J.-L. Redelsperger, A. Agusti-Panareda and A. Beljaars, 2010: The West African Monsoon water cycle. Part II: assessment of NWP models, J. Geophys. Res., doi:10.1029/2010JD013919 (in press).

Nguyen, H., C.D. Thorncroft, and C. Zhang, 2010: Coastal rainfall onset in the West African monsoon. *J. Clim.*, to be submitted.

Nicholson, S. E. and P.J. Webster, 2007: A physical basis for the interannual variability of rainfall in the Sahel. *Quart. J. Roy. Meteor. Soc.*, **133**, 2065-2084.

Nolan, D.S., C. Zhang, and S.h. Chen, 2007: Dynamics of the Shallow Meridional Circulation around Intertropical Convergence Zones. *J. Atmos. Sci.*, **64**, 2262–2285.

Okumura, Y., and S.P. Xie, 2004: Interaction of the Atlantic Equatorial Cold Tongue and the African Monsoon. *J. Climate*, **17**, 3589–3602.

Parker, D., C.D. Thorncroft, R. Burton, and A. Diongue-Niang, 2005: Analysis of the African easterly jet using aircraft observations from the JET2000 experiment. *Q.J.R. Meteorol. Soc.*, **131**, 1461-1482.

Peyrillé, P., and J.P. Lafore, 2007: An Idealized Two-Dimensional Framework to Study the West African Monsoon. Part II: Large-Scale Advection and the Diurnal Cycle. *J. Atmos. Sci.*, **64**, 2783-2803.

Polo, I., Lazar, A., Rodriguez-Fonseca, B. and Arnault, S. 2008: Oceanic Kelvin waves and tropical Atlantic intraseasonal variability: 1. Kelvin wave characterization. J. Geophys. Res., 113, CO7009, doi: 1029/2007/JC004495.

Pu, B. and K. H. Cook, 2010: Dynamics of the West African westerly jet, J. Clim. (submitted).

Ramel, R., H. Gallée and C. Messager, 2006: On the northward shift of the West African monsoon. *Clim. Dyn.*, **26**, 429-440.

Rienecker, Michele, M. Suarez, R. Gelaro, J. Bacmeister, R. Todling, L. Takacs, E. Liu, S. Pawson, M. Bosilovich, S. Schubert, G. Kim, et al., 2009. MERRA - NASA's Reanalysis, Overview of the System. *89th Annual Meeting of the AMS*.

Rodwell, M.J., and B.J. Hoskins, 2001: Subtropical Anticyclones and Summer Monsoons. *J. Climate*, **14**, 3192–3211.

Schumacher, C., R.A. Houze Jr. and I. Kraucunas, 2004: The Tropical Dynamical Repsonse to Latent Heating Estimates Derived from the TRMM Precipitation Radar, J. Atmos. Sci., 61, 1341-1358.

Sultan, B. and S. Janicot, 2000: Abrupt shift of the ITCZ over West Africa and intra-seasonal variability. *Geophys. Res. Lett.*, **27**, 3353-3356.

Schubert, W.H., P.E. Ciesielski, D.E. Stevens, and H.C. Kuo, 1991: Potential Vorticity Modeling of the ITCZ and the Hadley Circulation. *J. Atmos. Sci.*, **48**, 1493–1509.

Sijikumar, S., P. Roucou and B. Fontaine, 2006: Monsoon onset over Sudan-Sahel: Simulation by the regional scale model MM5. *Geophys. Res. Lett.*, **33**, L03814, doi:10.1029/2005GL024819.

Sultan, B. and S. Janicot, 2003: The West African Monsoon Dynamics. Part II: The "Preonset" and "Onset" of the Summer Monsoon. *J. Climate*, **16**, 3407–3427.

Thorncroft, C.D. and M. Blackburn, 1999: Maintenance of the African easterly jet. *Q.J.R.Meteorol. Soc.*, **125**, 763-786.

Tomas, R. and P. J. Webster, 1997: The role of inertial instability in determining the location and strenght of near-equatorial convection. *Quar. J. Roy. Met. Soc.*, **123**, 1445-1482.

Uppala and Coauthors, 2005: The ERA-40 re-analysis. *Quar. J. Roy. Met. Soc.*, **131**, 2961-3012.

Xie, P and Arkin, P.A., 1997: Global Precipitation: A 17-Year Monthly Analysis Based on Gauge Observations, Satellite Estimates, and Numerical Model Outputs, Bull. Amer. Meteorol. Soc. 1997; 78: 2539-2558

Xie, P., J.E. Janowiak, P.A. Arkin, R. Adler, A. Gruber, R. Ferraro, G.J. Huffman, and S. Curtis, 2003: GPCP Pentad Precipitation Analyses: An Experimental Dataset Based on Gauge Observations and Satellite Estimates. *J. Climate*, **16**, 2197–2214.

Zhang, C., and S.M. Hagos, 2009: Bi-Modal Structure and Variability of Large-Scale Diabatic Heating in the Tropics. *J. Atmos. Sci*., 66, 3621-3640.

Zhang, C., D.S. Nolan, C.D. Thorncroft, and H. Nguyen, 2008: Shallow Meridional Circulations in the Tropical Atmosphere. *J. Climate*, **21**, 3453–3470.

Zhang, C., P. Woodworth, and G. Gu, 2006: The seasonal cycle in the lower troposphere over West Africa from sounding observations. Q. J. Roy. Meteorol. Soc., 132, 2561-2584.

Zheng, X., Eltahir, E.A.B. and Emanuel, A.K. 1999 A mechanism relating tropical Atlantic spring sea surface temperature and west African rainfall. *Quart. J. Roy. Meleorol. Soc.*, **125**, 1129-1163.

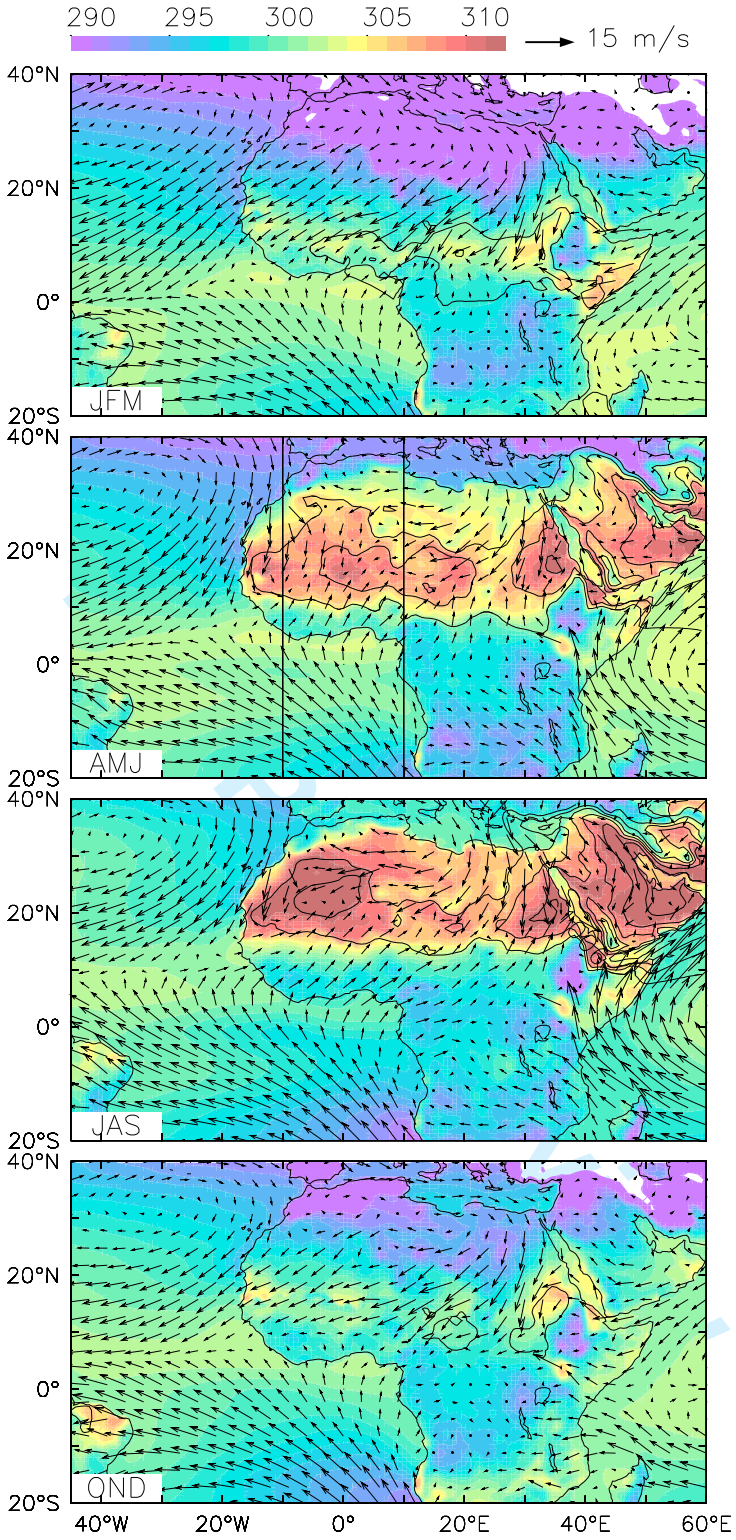

Figure 1: ERA-Interim seasonally mean (1979-2001) 925 hPa wind (vectors, m s^{-1}) and surface skin temperature (shading, degK). Mean sea level pressure contours lower than 1010 hPa are superimposed (contour interval 2 hPa). The two vertical lines in second panel indicate the zonal limit used thereafter.

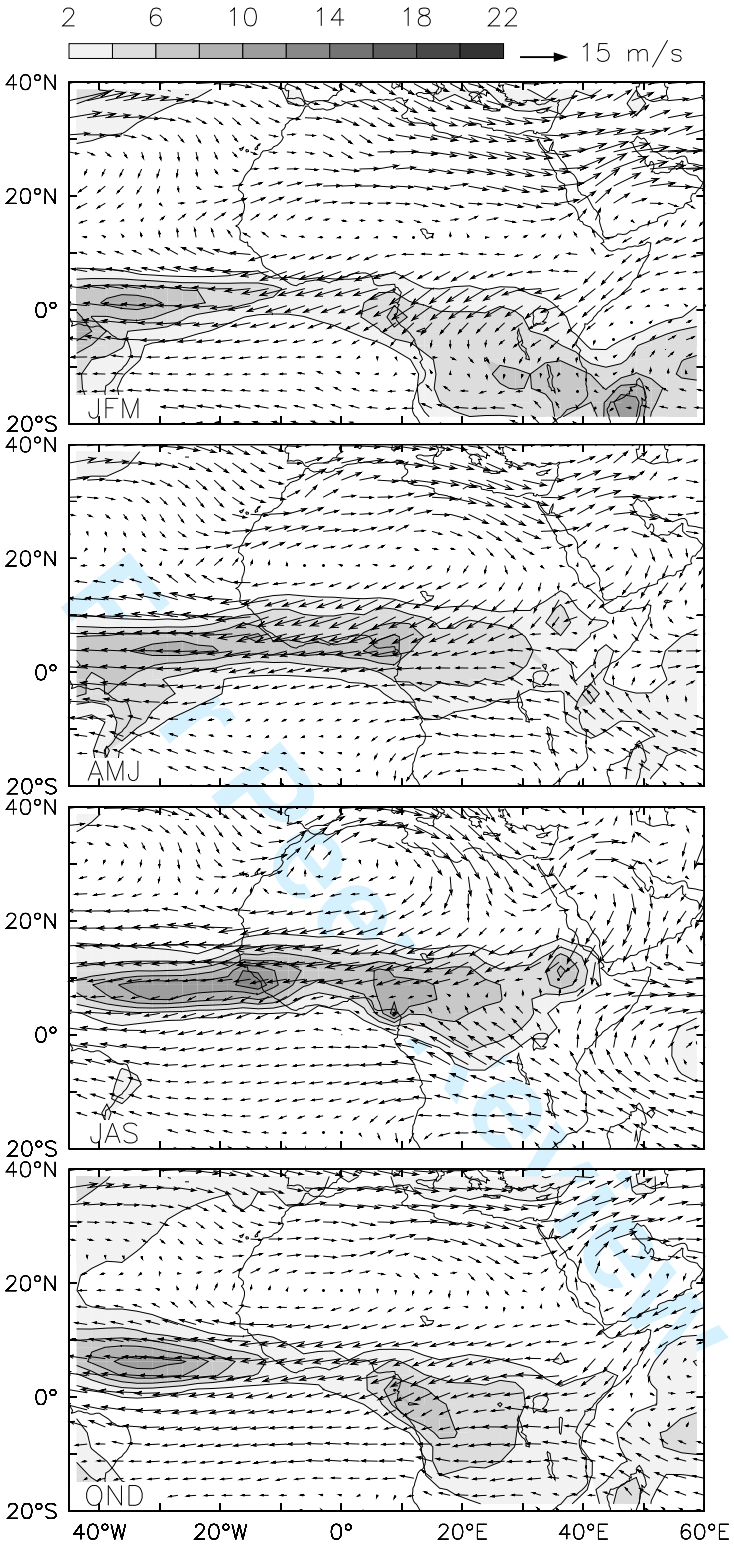

Figure 2: Seasonally mean ERA-Interim 700 hPa wind (vectors, m s^{-1}) and GPCP precipitation (shading, mm d^{-1}).

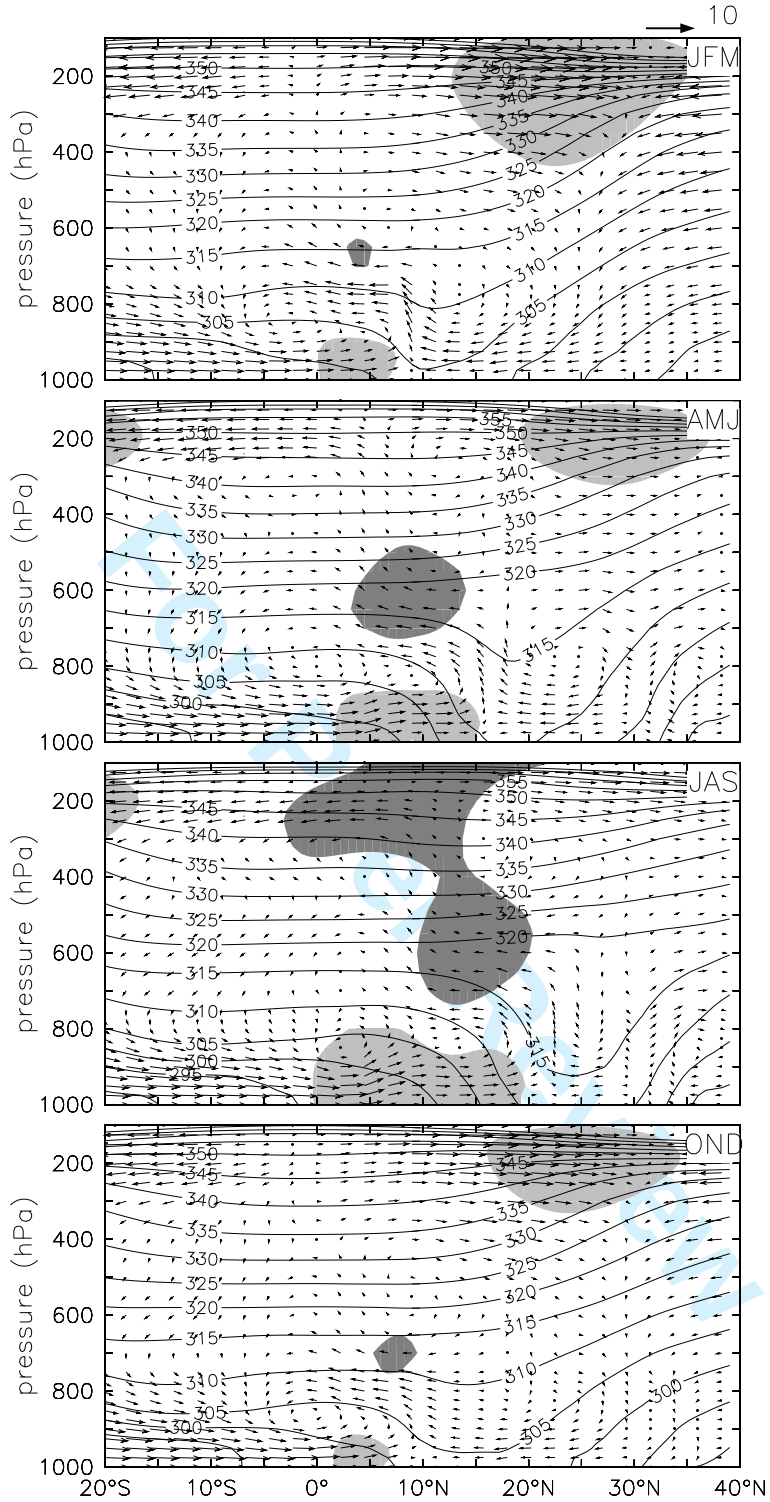

Figure 3: Vertical cross-section of ERA-Interim (10°W-10°E) zonal mean meridional circulation (vectors, horizontal velocity is expressed as m s^{-1} and vertical velocity is multiplied by -20 Pa s^{-1}) and potential temperature (contour interval 5 K). Shadings indicate westerly (monsoonal trade and tropospheric jet, light grey) and easterly (AEJ, dark grey) wind (m s^{-1}).

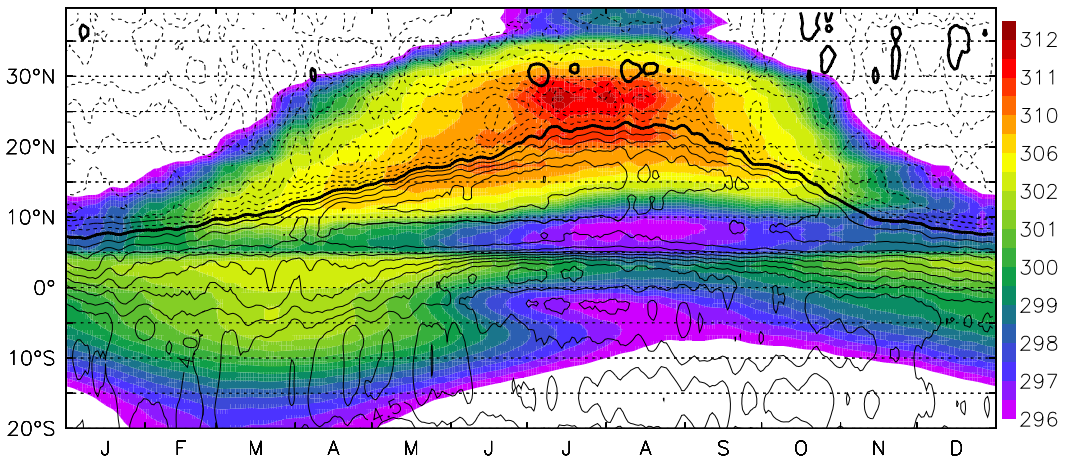

(a) SKT and V_{10m}

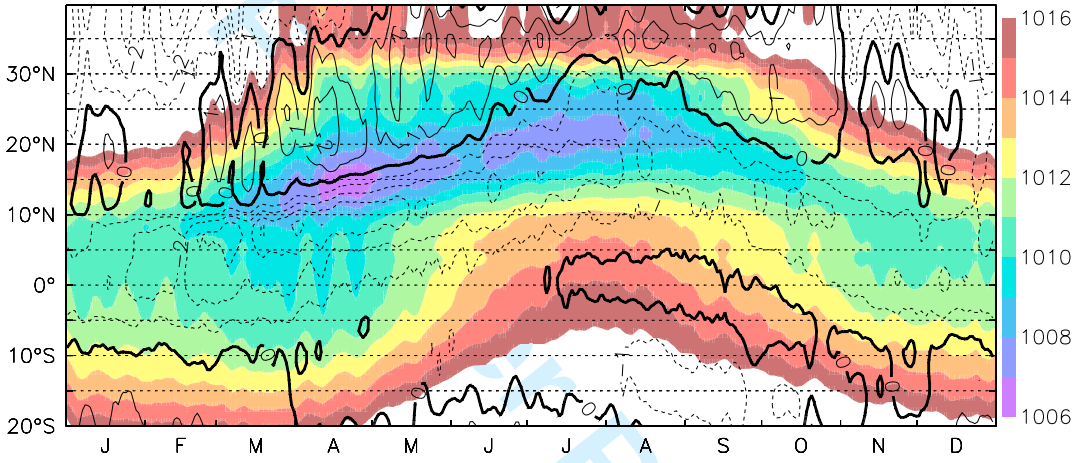

(b) MSLP and V_{700hPa}

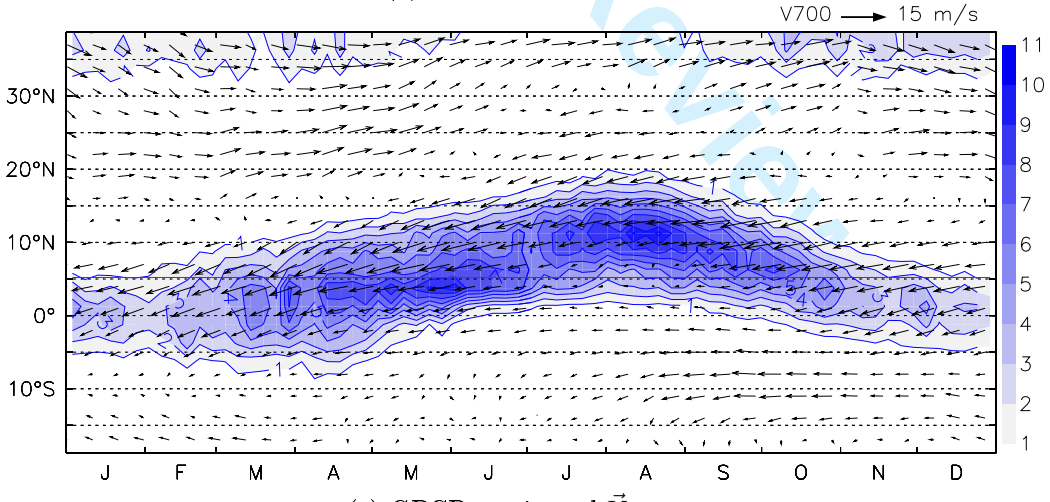

(c) GPCP precip and $\vec{V}_{700hPa}$

Figure 4: Hovmoeller diagrams of ERA-Interim (10°W-10°E) zonal mean (a) surface temperature (shading interval 1 K from 296 to 300 K then 2 K) and meridional 10 m wind (contour interval 0.5 m s^{-1}), (b) mean sea level pressure (MSLP, shading interval 0.5 hPa from 296 to 302 then 2 hPa) and 700 hPa meridional wind (contour interval 1 m s^{-1}) and (c) GPCP precipitation (shading interval 2 mm d^{-1}) and 700 hPa wind (vector, m s^{-1}). Red line represents the average coastal limit.

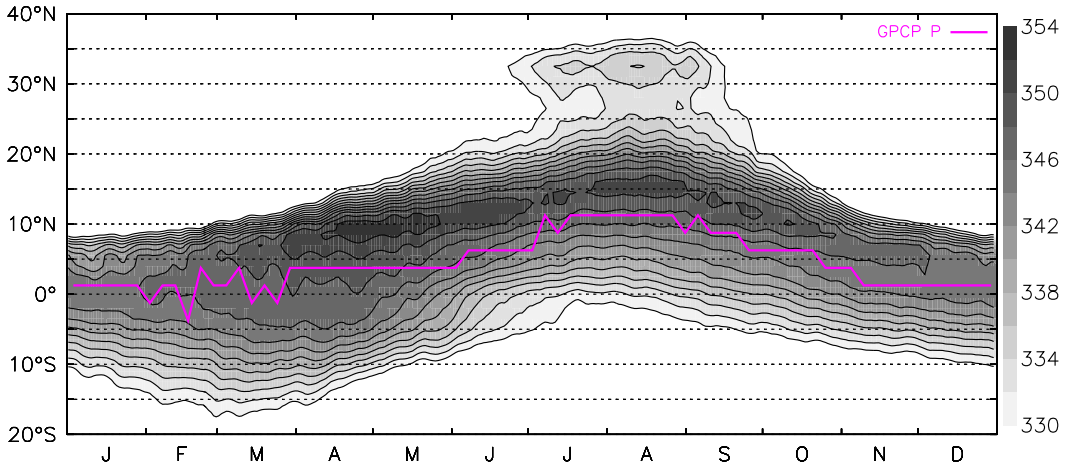

Figure 5: Hovmoeller diagrams of ERA-Interim (10°W-10°E) zonal mean equivalent potential temperature at 925 hPa (K). The position of the peak in rainfall from GPCP (purple curve) is superimposed.

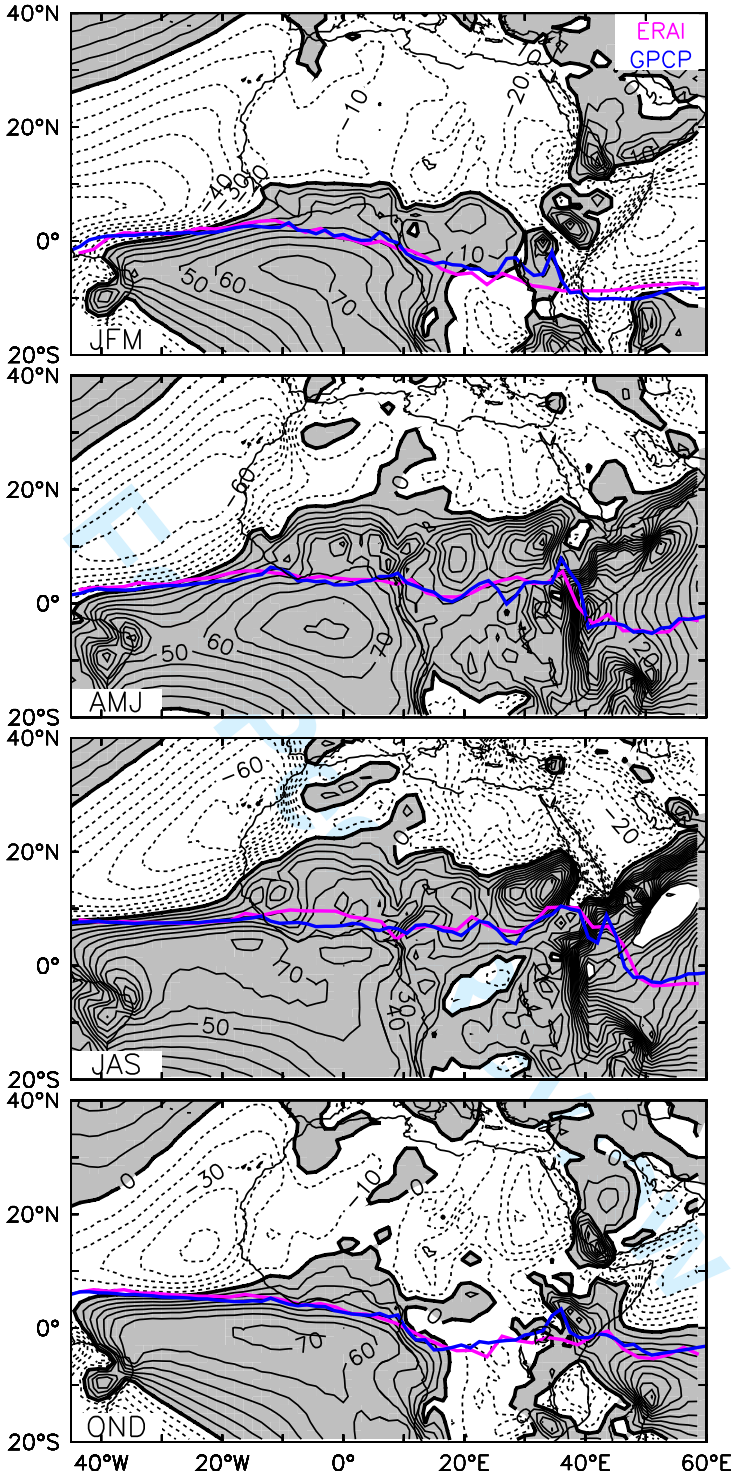

Figure 6: ERA-Interim seasonally mean of vertically integrated meridional moisture flux from the 1000 to 850 hPa. Southerly fluxes are shaded (contour interval 10 kg m^{-1} s^{-1}). Blue (purple) contour highlights the peak rainfall from ERA-Interim (GPCP).

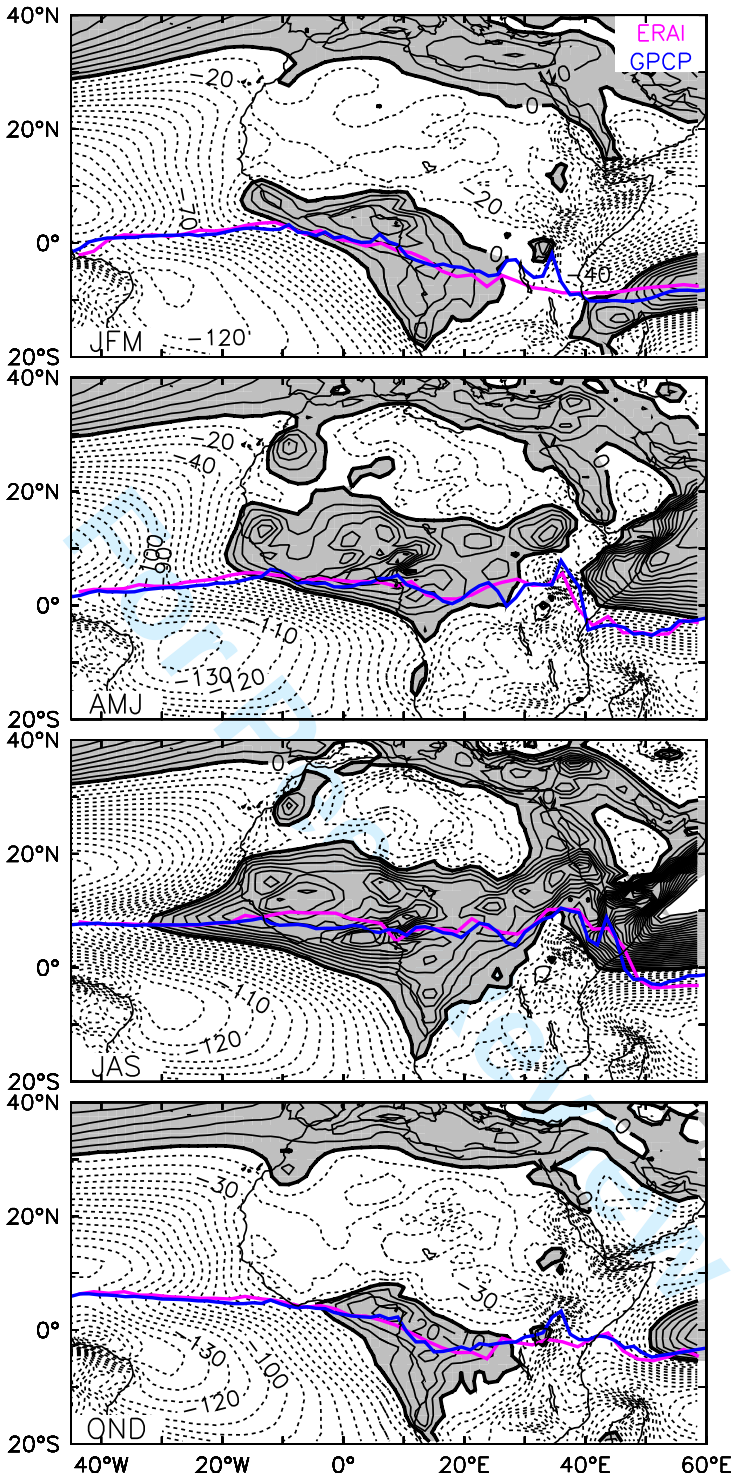

Figure 7: As in Figure 6 except for the zonal component. Westerly fluxes are shaded.

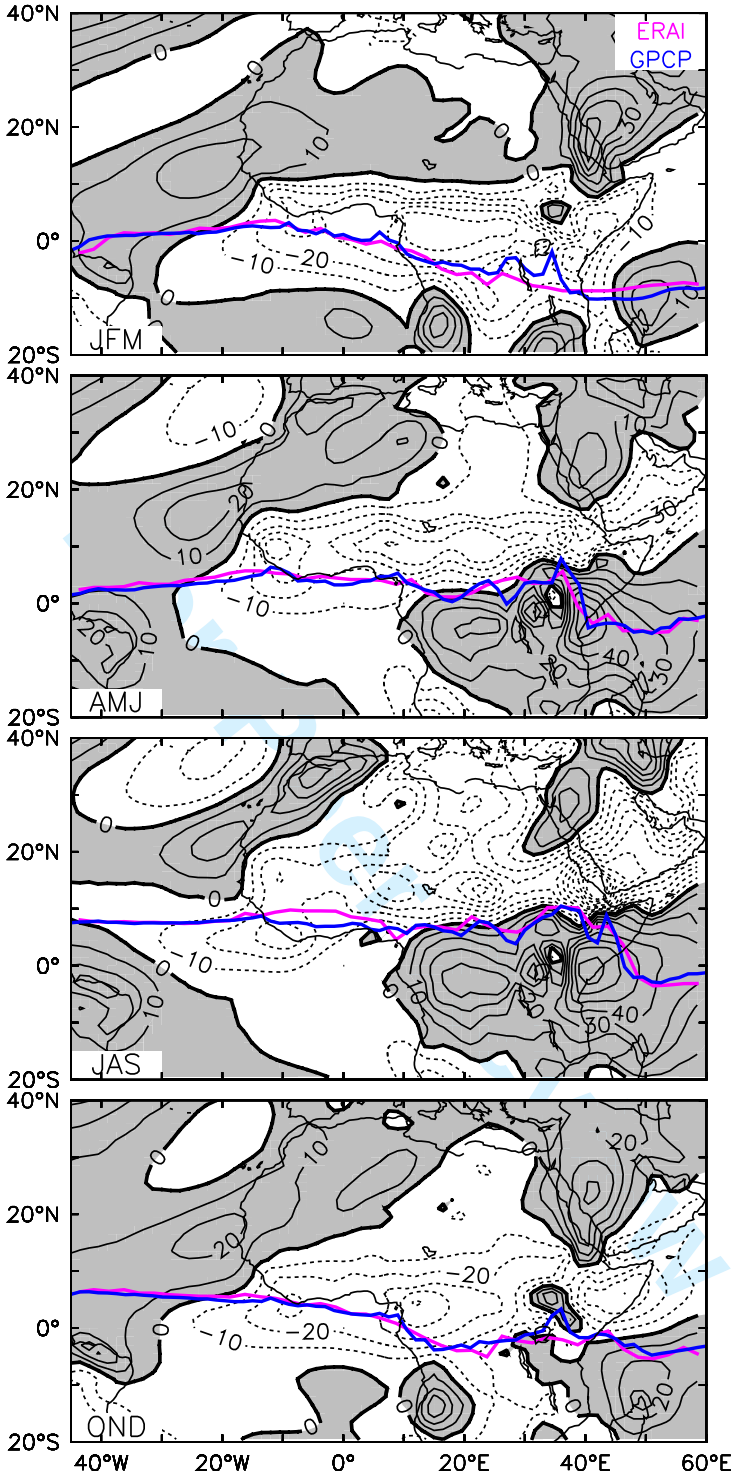

Figure 8: As in Figure 6 except for the 825-500 hPa layer.

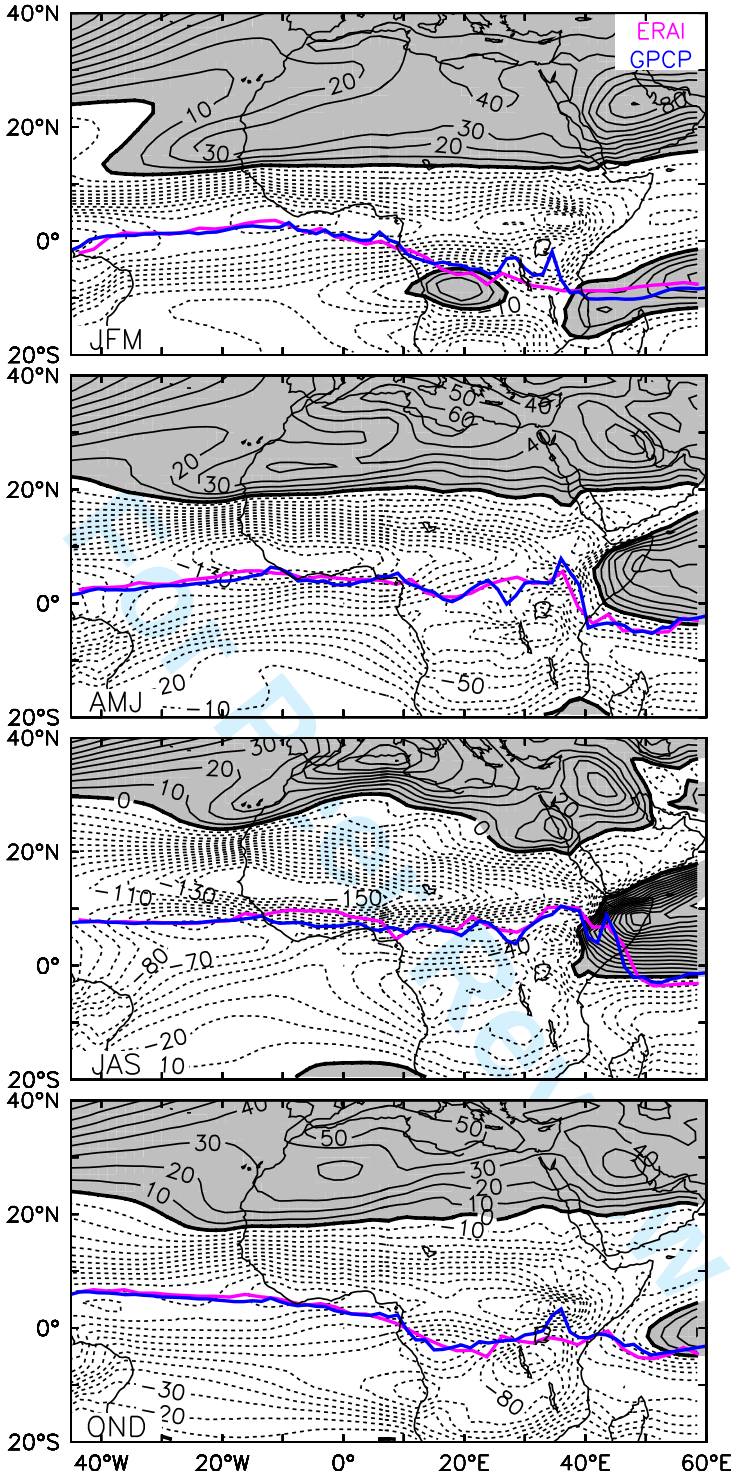

Figure 9: As in Figure 8 except for the zonal component.

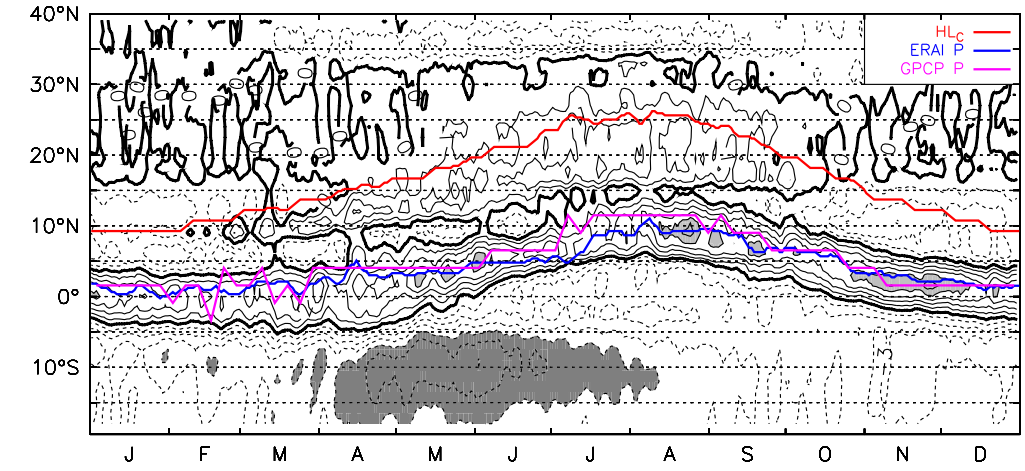

(a) total column flux convergence

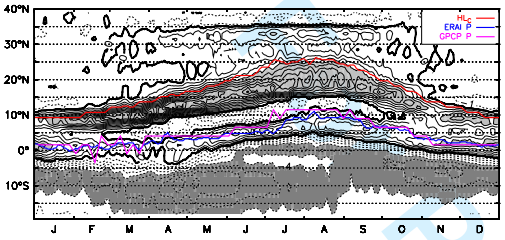

(b) low-level flux convergence

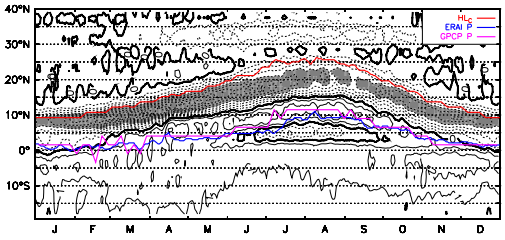

(c) mid-level flux convergence

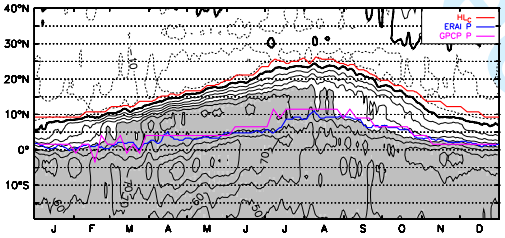

(d) low-level meridional flux

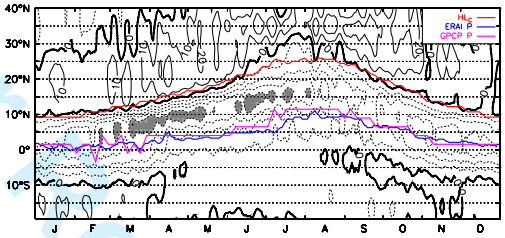

(e) mid-level meridional flux

Figure 10: Hovmoeller diagrams of (10°W-10°E) zonal mean moisture flux convergence (contour interval 1 mm d^{-1}, absolute values greater than 4 mm d^{-1} are shaded) integrated on (a) total column (from 1000 to 100 hPa), (b) low-levels (from 1000 to 850 hPa) and (c) mid-levels (from 825 to 500 hPa). Meridional moisture flux (contour interval 10 kg m^{-1} s^{-1}, absolute values greater than 40 kg m^{-1} s^{-1} are shaded) at (d) low-levels and (e) and mid-levels. Zero contour is bold. The position of the HL center (red curve) peak rainfall from GPCP (purple curve) and from ERA-Interim (blue curve) are superimposed.

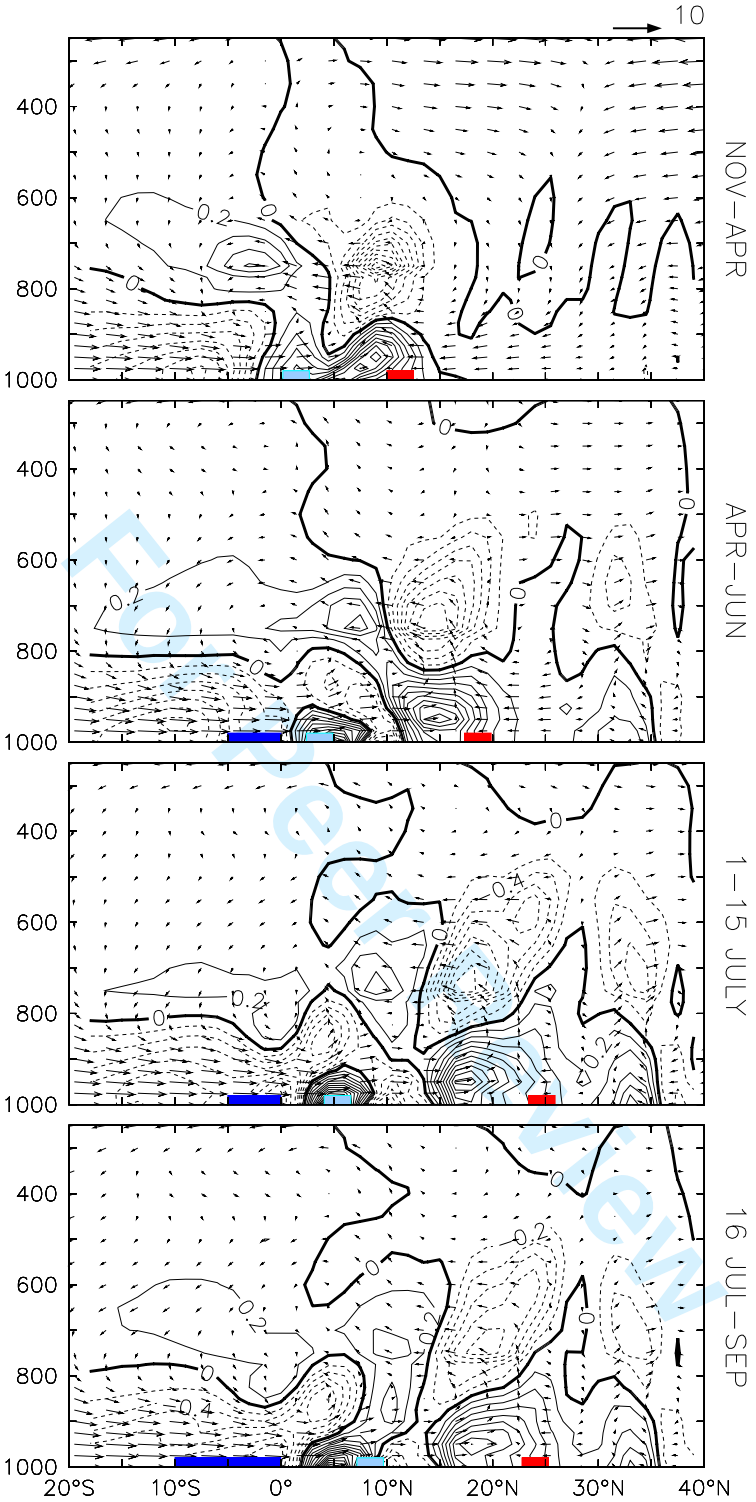

Figure 11: Vertical cross-section of ERA-Interim (10°W-10°E) zonal mean moisture flux convergence (contour interval 0.5 mm d^{-1}) and meridional circulation (vectors, horizontal velocity is expressed as m s^{-1} and vertical velocity is multiplied by -20 Pa s^{-1}). The light blue and red boxes indicates the latitude of rainfall peak and heat low, respectively. The dark blue box represents the extension of the Atlantic cold tongue.

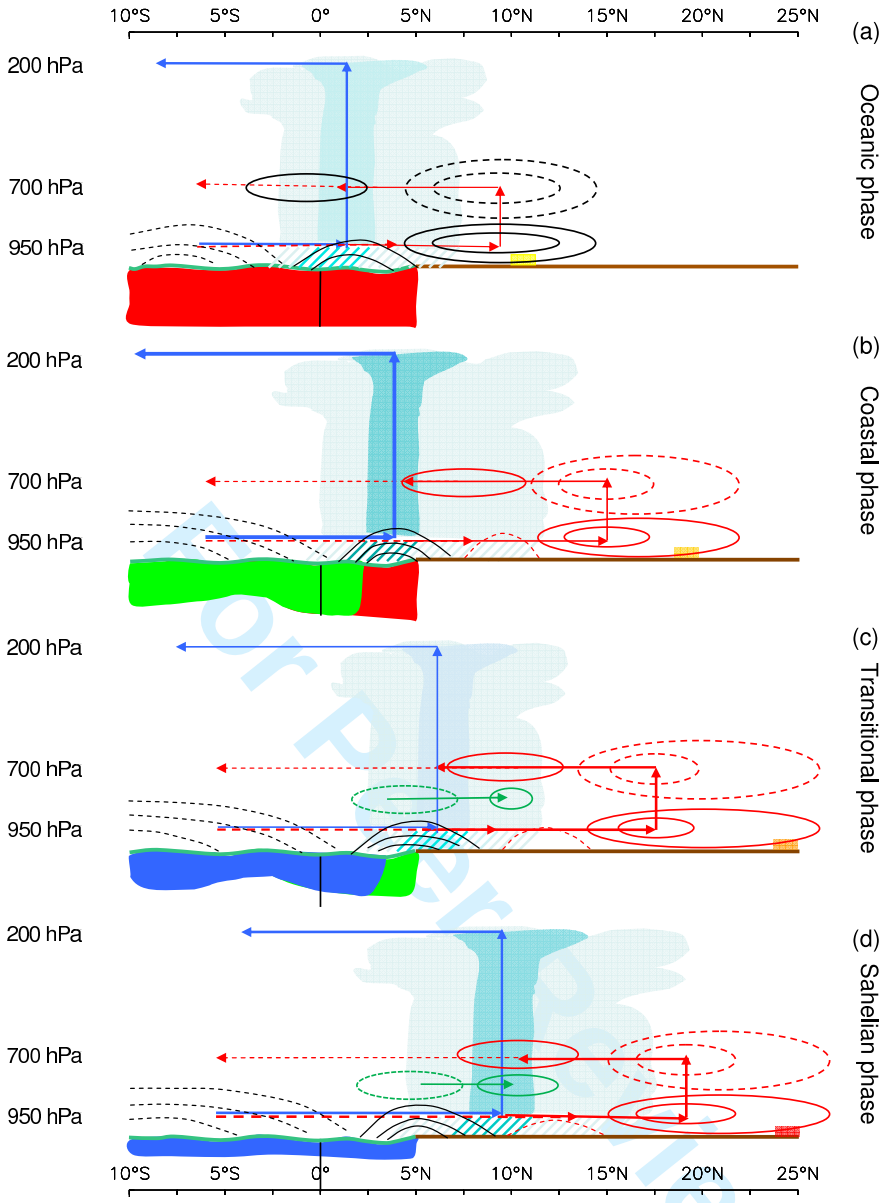

Figure 12: Schematic showing the four key phases of the Annual cycle of the West African monsoon. Included for each phase are the following: the location of the main rainband (indicated by clouds and rainfall with peak values highlighted by darker shaded clouds and rainfall), the location of the Saharan heat low (indicated by yellow, orange and red shading at the surface poleward of the rainband, with increased redness indicating increased intensity), Atlantic ocean temperature and associated mixed-layer depth (with decreased tempereatures indicated by the red-to-green-to-blue transition), moisture flux convergence maxima and minima (solid contours indicate moisture flux convergence and dashed contours indicate moisture flux divergence), and the deep and shallow meridional circulations (blue and red lines with arrows; dashed lines suggest some uncertainty about the extent to which SMC return flow penetrates the latitude of the main rainband or not. The moisture flux convergence quadrapole structure is highlighted by red contours and the dipole at 850hPa structure is highlighted by green contours. See text for more details.

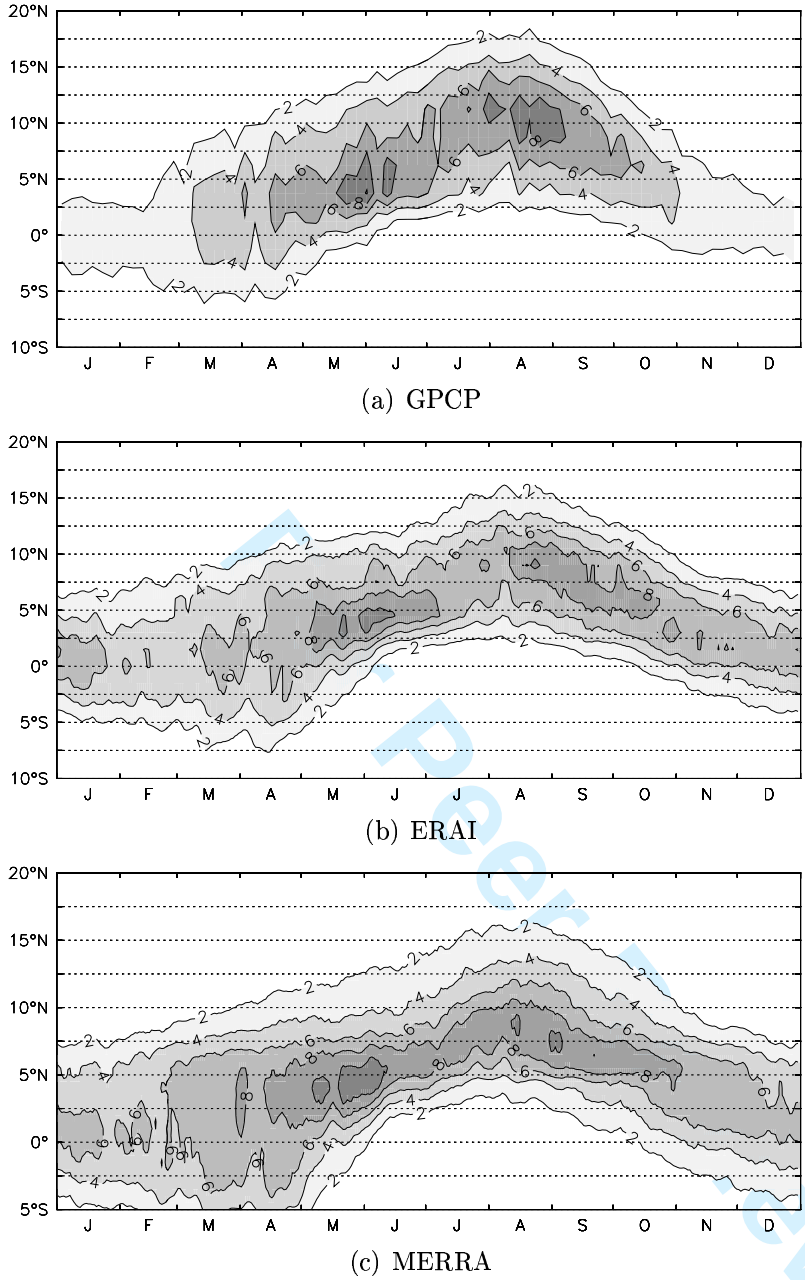

(a) GPCP

(b) ERAI

(c) MERRA

Figure A-1: Hovmoeller diagrams of (10°W-10°E) zonal mean precipitation (mm d^{-1}) from (a) GPCP, (b) ERA-Interim and (c) MERRA.

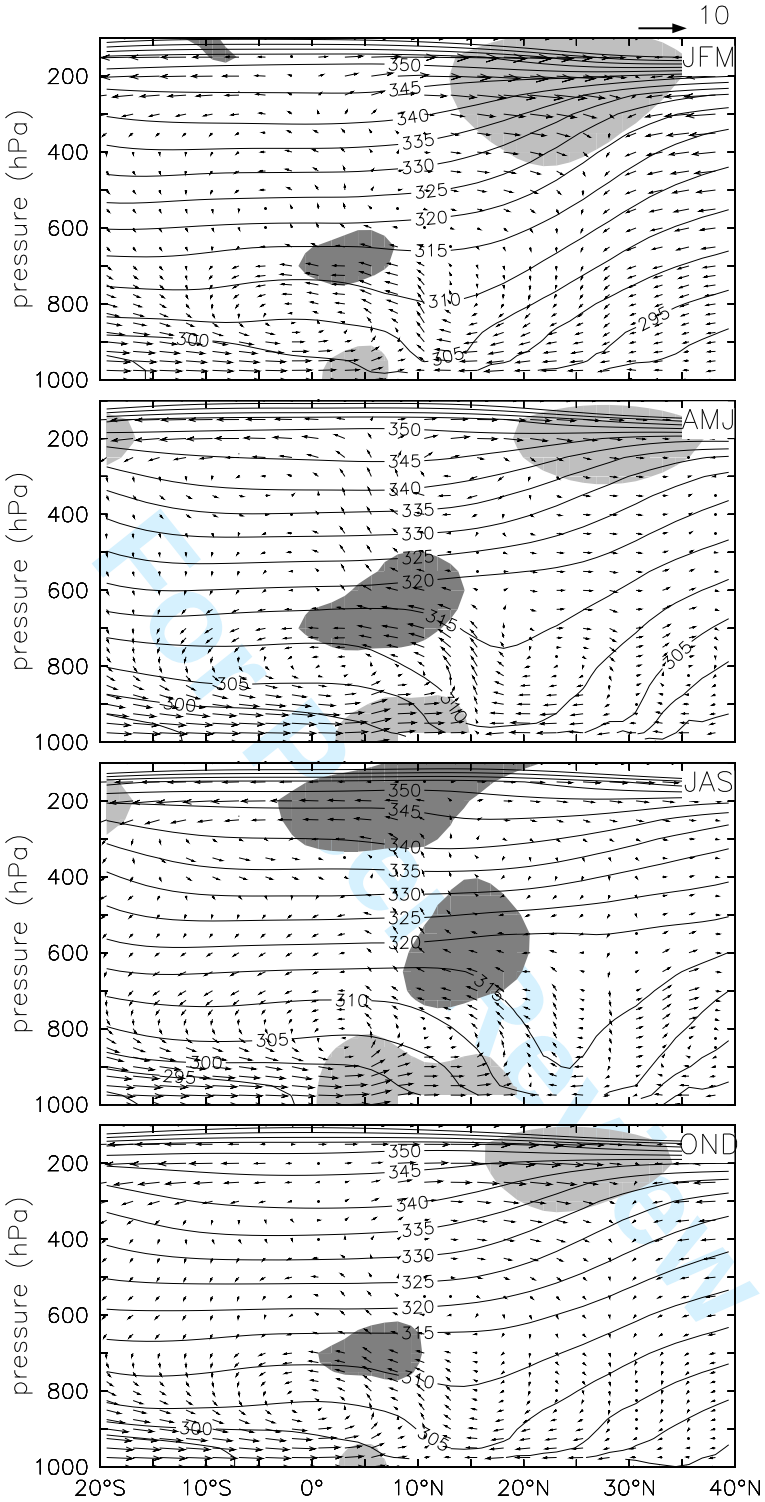

Figure A-2: As in Fig.3 except for MERRA reanalysis data.

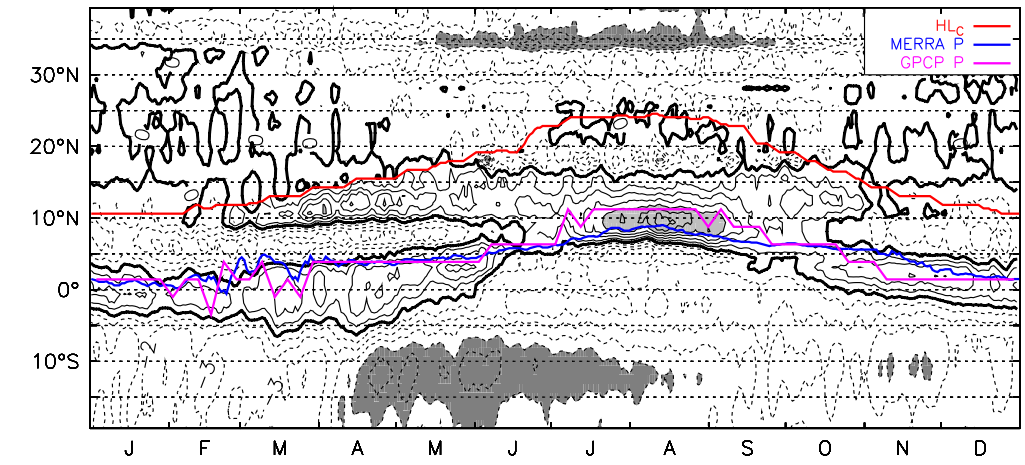

(a) total column flux convergence

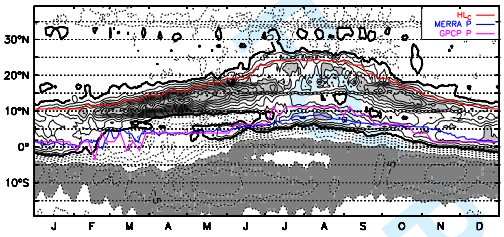

(b) low-level flux convergence

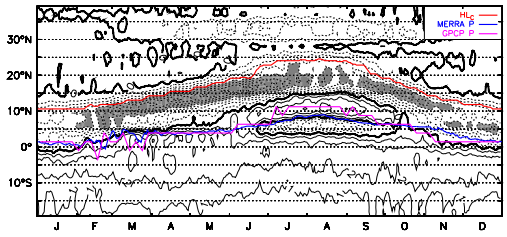

(c) mid-level flux convergence

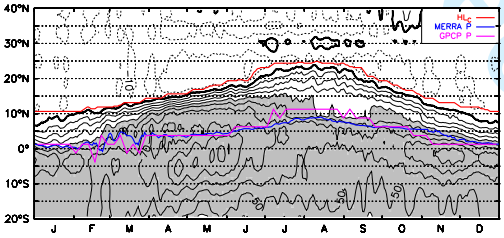

(d) low-level meridional flux

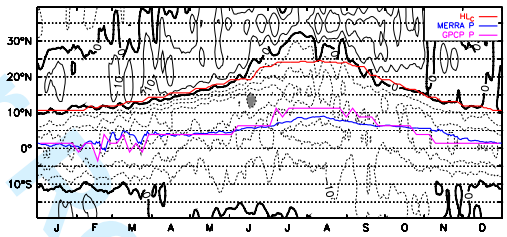

(e) mid-level-level meridional flux

Figure A-3: As in Fig.10 except for MERRA reanalysis data.

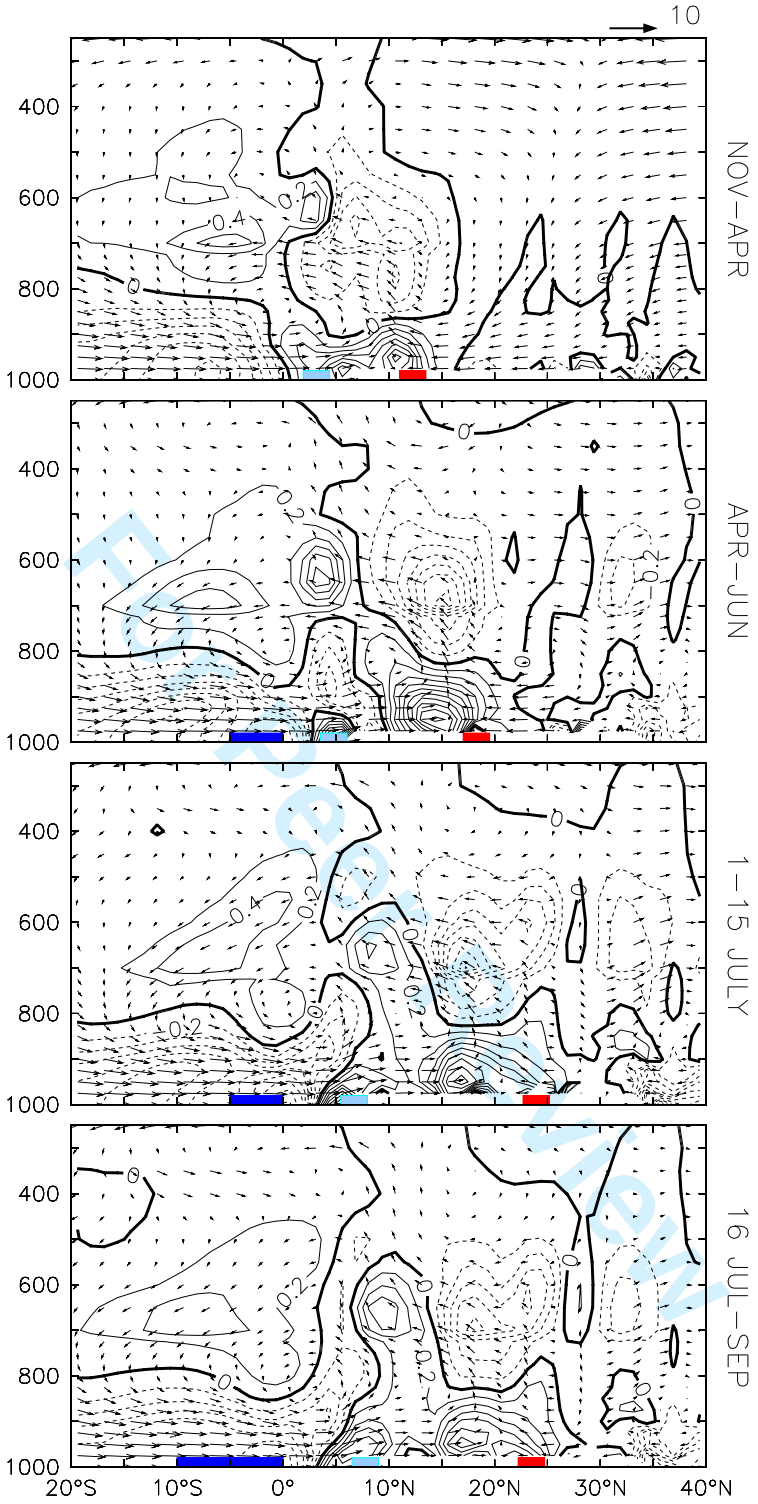

Figure A-4: As in Fig.11 except for MERRA reanalysis data.